

1 A manuscript submitted to discussion forum of BG as a BG discussion paper(bg-2016-222):

2 **Revised according to the reviewer's comments (RC) 3**

3

4

5 Manganese and iron reduction dominate organic carbon oxidation in surface  
6 sediments of the deep Ulleung Basin, East Sea

7

8

9 Jung-Ho Hyun<sup>1\*</sup>, Sung-Han Kim<sup>1</sup>, Jin-Sook Mok<sup>1</sup>, Hyeyoun Cho<sup>1</sup>, Tongsup Lee<sup>2</sup>, Verona  
10 Vandieken<sup>3</sup> and Bo Thamdrup<sup>4\*</sup>

11

12

13 <sup>1</sup>Department of Marine Sciences and Convergent Technology, Hanyang University, 55  
14 Hanyangdaehak-ro, Ansan, Gyeonggi-do 15588, South Korea

15

16 <sup>2</sup>Department of Oceanography, Pusan National University, Busan 609-735, South Korea

17

18 <sup>3</sup>Institute for Chemistry and Biology of the Marine Environment, University of Oldenburg,  
19 Carl-von-Ossietzky-Str. 9-11, 26129 Oldenburg, Germany

20

21 <sup>4</sup>Nordic Center for Earth Evolution, Department of Biology, University of Southern Denmark,  
22 Campusvej 55, 5230 Odense M, Denmark

23

24

25 \*Correspondence to:

26 Jung-Ho Hyun ([hyunjh@hanyang.ac.kr](mailto:hyunjh@hanyang.ac.kr))

27 Bo Thamdrup ([bot@biology.sdu.dk](mailto:bot@biology.sdu.dk))

28

29

30

31 **Abstract.** Rates and pathways of benthic organic carbon ( $C_{\text{org}}$ ) oxidation were investigated in  
32 surface sediments of the Ulleung Basin (UB) characterized by high organic carbon contents ( $>$   
33 2.5 %, dry wt.) and very high contents of Mn oxides ( $> 200 \mu\text{mol cm}^{-3}$ ) and Fe oxides (up to  
34  $100 \mu\text{mol cm}^{-3}$ ). The combination of geochemical analyses and independently executed  
35 metabolic rate measurements revealed that Mn and Fe reduction were the dominant  $C_{\text{org}}$   
36 oxidation pathways in the center of the UB, comprising 45 % and 20 % of total  $C_{\text{org}}$  oxidation,  
37 respectively. By contrast, sulfate reduction was the dominant  $C_{\text{org}}$  oxidation pathway  
38 accounting for 50 % of total  $C_{\text{org}}$  mineralization in sediments of the continental slope. The  
39 relative significance of each  $C_{\text{org}}$  oxidation pathway matched the depth distribution of the  
40 respective electron acceptors. The relative importance of Mn reduction for  $C_{\text{org}}$  oxidation  
41 displays saturation kinetics with respect to Mn oxide content with a low half-saturation value  
42 of  $8.6 \mu\text{mol cm}^{-3}$ , which further implies that Mn reduction can be a dominant  $C_{\text{org}}$  oxidation  
43 process even in sediments with lower  $\text{MnO}_2$  content as known from several other locations.  
44 This is the first report of a high contribution of manganese reduction to  $C_{\text{org}}$  oxidation in  
45 offshore sediments on the Asian margin. The high manganese oxide content in the surface  
46 sediment in the central UB was maintained by an extreme degree of recycling, with each Mn  
47 atom on average being reoxidized  $\sim 3800$  times before permanent burial. This is the highest  
48 degree of recycling so far reported for Mn-rich sediments, and it appears linked to the high  
49 benthic mineralization rates resulting from the high organic carbon content that indicate the  
50 UB as a biogeochemical hotspot for turnover of organic matter and nutrient regeneration.  
51 Thus, it is important to monitor any changes in the rates and partitioning of  $C_{\text{org}}$  oxidation to  
52 better understand the biogeochemical cycling of carbon, nutrients and metals associated with  
53 long-term climatic changes in the UB, where the gradual deoxygenation and warming of the  
54 bottom water have resulted in an  $\sim 10\%$  decrease in dissolved oxygen and  $\sim 0.04 \text{ }^\circ\text{C}$   
55 increase in potential temperature for the past three decades.

56  
57

58 **Keywords.** Benthic mineralization, Manganese reduction, Iron reduction, Sulfate reduction,  
59 Ulleung Basin, East Sea

60  
61  
62  
63

## 64 **1 Introduction**

65

66 Although they cover only 15 % ( $47 \times 10^6 \text{ km}^2$ ) of the ocean surface area, sediments of  
67 continental margins (200 – 2000 m depth) are characterized by enhanced organic matter flux  
68 generated either by vertical transport from the highly productive overlying water column or  
69 by lateral transport from adjacent shelves, and thus play an important role in deposition and  
70 mineralization of organic matter (Romankevich, 1984, Jahnke et al., 1990; Walsh, 1991;  
71 Jahnke and Jahnke, 2000). Organic particles that reach the seafloor are quickly mineralized  
72 by hydrolysis, fermentation, and a variety of respiratory processes using different electron  
73 acceptors such as oxygen, nitrate, Mn oxides, Fe oxides, and sulfate (Froelich et al., 1979;  
74 Jørgensen, 2006). The partitioning of organic carbon ( $C_{\text{org}}$ ) oxidation among the different  
75 electron accepting pathways has profound influence on the distribution and the release and/or  
76 retention of Mn, Fe, S and nutrients (nitrogen and phosphate) (Canfield et al., 2005; Hansen et  
77 al., 2006; Jørgensen, 2006; Slomp et al., 2013). Therefore, it is particularly important to  
78 elucidate the contribution of each  $C_{\text{org}}$  oxidation pathway in order to better understand the  
79 role of sediments in biogeochemical element cycles.

80 The relative significance of each carbon oxidation pathway is largely controlled by the  
81 combination of organic matter supply and availability of electron acceptors. In general,  
82 aerobic metabolism dominates the organic matter mineralization in deep-sea sediments that  
83 are characterized by low organic matter content (Jahnke et al., 1982; Glud, 2008), especially  
84 in organic carbon-starved deep-sea sediments with low sedimentation rates (Mewes et al.,  
85 2014, 2016; D'Hondt et al. 2015; Mogollón et al., 2016). In contrast, owing to high sulfate  
86 concentrations in marine sediment, sulfate reduction might account for up to 50% of total  
87 carbon oxidation in continental margins with high organic matter flux (Jørgensen, 1982;  
88 Jørgensen and Kasten, 2006; Bowles et al., 2014). However, in sediments where manganese  
89 and iron oxides are abundant or rapidly recycled, microbial reduction of manganese and iron  
90 can be the dominant electron accepting processes over sulfate reduction (Sørensen and  
91 Jørgensen, 1987; Aller, 1990; Canfield et al., 1993b). The significance of dissimilatory iron  
92 reduction for  $C_{\text{org}}$  oxidation is well established in the sediments of various continental  
93 margins and coastal wetlands (Thamdrup, 2000; Thamdrup and Canfield, 1996; Jensen et al.  
94 2003, Kostka et al., 2002a, 2002b; Vandieken et al., 2006; Hyun et al., 2007, 2009b).  
95 However, only a few locations such as the Panama Basin (Aller, 1990), the coastal  
96 Norwegian trough in Skagerrak and an adjacent fjord (Canfield et al., 1993a, 1993b;

97 Vandieken et al., 2014), the Black Sea shelf (Thamdrup et al., 2000) and the continental shelf  
98 of the northern Barents Sea (Vandieken et al., 2006; Nickel et al., 2008) are known where  
99 microbial manganese reduction significantly contributes to carbon mineralization.

100 The East Sea (often referred to as Japan Sea), located in the far eastern part of the Eurasian  
101 continental margin, consists of three major basins deeper than 2000 m, the Japan Basin, the  
102 Yamato Basin and the Ulleung Basin (Fig. 1). Compared to the other two basins, the surface  
103 waters of the Ulleung Basin (UB) are characterized by higher phytoplankton biomass and  
104 primary production (Yamada et al., 2005; Yoo and Park, 2009), which is associated with  
105 coastal upwelling (Hyun et al., 2009a). The enhanced biological production in the euphotic  
106 zone of the UB is responsible for the high organic carbon content ( $> 2.5$  % wt) in the  
107 sediment, and the highest rates of  $C_{org}$  oxidation compared to other deep-sea sediments with  
108 similar depth range (Lee et al., 2008; Hyun et al., 2010). An intriguing geochemical property  
109 of the UB surface sediment is the high content of Mn oxides ( $>200 \mu\text{mol cm}^{-3}$ ) and Fe oxides  
110 (up to  $100 \mu\text{mol cm}^{-3}$ ) (Cha et al., 2007; Hyun et al., 2010). In accordance with these  
111 geochemical findings, the suppression of sulfate reduction (Hyun et al., 2010) and  
112 accumulation of  $\text{Mn}^{2+}$  in anoxic incubation of surface sediment (Vandieken et al., 2012)  
113 strongly implied that the  $C_{org}$  oxidation in the surface sediment of the UB is dominated by  
114 microbial manganese and iron reduction, but actual rates and partitioning of each electron  
115 accepting pathway in  $C_{org}$  oxidation remain to be determined in this deep marginal sediment  
116 underlying highly productive surface waters.

117 The primary objective of this paper was to characterize the sediment biogeochemistry with  
118 regard to the rate of  $C_{org}$  oxidation and partitioning of major terminal electron accepting  
119 pathways at two contrasting sites at the continental slope and rise in the UB. Here, for the  
120 first time in sediments of the Asian marginal seas, we document that Mn and Fe reduction are  
121 the dominant  $C_{org}$  oxidation pathways accounting for respectively 45% and 20% of total  $C_{org}$   
122 oxidation in the center of the UB, and suggest that Mn and Fe reduction may be of greater  
123 importance in deep-sea sediments than previously recognized.

124

## 125 **2 Materials and methods**

126

### 127 **2.1 Studysite**

128

129 The East Sea is a marginal sea surrounded by the east Asian continent and Japanese Islands

130 (Fig.1, Kang et al., 2010; Liu et al., 2010). The UB located in the southwestern part of the  
131 East Sea is a bowl-shaped deep basin (2000 – 3000 m depth) (Fig. 1) delimited by continental  
132 slopes of Korean Peninsula and the southwestern Japanese Archipelago on the west and south,  
133 respectively, and by the Korea Plateau and the Oki Bank on the north and east, respectively  
134 (Chough et al., 2000).

135 Shipboard experiments were conducted in June, 2009 at two sites on the continental slope  
136 (Station M1, hereafter M1) and in the center (Station D3, hereafter D3) of the the UB (Fig. 1,  
137 Table 1). Surface sediments consist of fine-grained clay with a mean grain size less than  
138 0.004 mm in diameter (Cha et al., 2007). Two stations were characterized by two contrasting  
139 sediment colors. The Mn oxide-enriched surface sediment at the basin site (D3) was reddish-  
140 brown, whereas at the slope site (M1) it exhibited the typical gray-brown color of muddy  
141 continental margin sediments (Fig. 1). Further environmental properties are listed in Table 1.

142

## 143 **2.2 Sampling and handling**

144

145 Sediment samples were collected with a box corer. Onboard, duplicate or mostly triplicate  
146 sub-samples for geochemical analyses were collected using acrylic cores (6–9 cm in diameter  
147 and 30–40 cm in length). The sub-cores for geochemical analyses were immediately sealed  
148 with butyl rubber stoppers and transferred to a N<sub>2</sub>-filled glove bag for sectioning and loading  
149 into polypropylene centrifuge tubes that were then tightly capped and centrifuged for 15 min  
150 at 5000 × g. After reintroduction into the N<sub>2</sub>-filled glove bag, pore-waters were sampled and  
151 filtered through 0.2-μm cellulose ester syringe filters (ADVANTEC, Toyo Rashi Kaisha, Ltd).  
152 One to two mL of pore water to determine NH<sub>4</sub><sup>+</sup> was fixed with saturated HgCl<sub>2</sub>, and frozen.  
153 For determination of Fe<sup>2+</sup>, Mn, SO<sub>4</sub><sup>2-</sup> and Ca<sup>2+</sup>, 2 mL of the pore water were acidified with  
154 12M HCl and stored at 4 °C. Pore-water for sulfide analysis was preserved with Zn acetate  
155 (20%). Sediments for solid-phase analysis were frozen at –25°C for future analyses.

156

## 157 **2.3 Anoxic bag incubations**

158

159 Anaerobic carbon mineralization rates and dissimilatory Mn and Fe reduction rates were  
160 determined in batch incubations based on the procedures of Canfield et al. (1993b) and  
161 Thamdrup and Canfield (1996). Sediment cores were transferred to a N<sub>2</sub>-filled glove bag and  
162 sliced in 2-cm intervals to a depth of 10 cm. Sediment from parallel sections was pooled,

163 mixed and loaded into gas-tight plastic bags (Hansen et al., 2000). The bags were sealed  
164 without gas space, and incubated in the dark at near in situ temperature (ca. 1 –2°C) in larger  
165 N<sub>2</sub> filled bags to ensure anoxic conditions. Over a period of 18 days of incubation, sub-  
166 samples to determine the accumulation of total dissolved inorganic carbon (DIC) and Mn in  
167 pore water were withdrawn on days 0, 1, 3, 5, 9 and 18. Two 50-mL centrifuge tubes per bag  
168 were filled completely with sediment in a N<sub>2</sub>-filled glove bag, and pore-water was extracted  
169 as described above. For DIC analysis, we collected 1.8 mL aliquots into glass vials without  
170 head space, fixed with 18 µL of HgCl<sub>2</sub> (125 mM), and stored at 4 °C until analysis within 4  
171 weeks. Samples for Mn analysis were acidified with 12 M HCl and stored at 4°C. Sediment  
172 remaining after the collection of pore water was frozen at –25°C for later analysis of oxalate  
173 extractable solid Fe(II).

174

## 175 **2.4 Pore-water analyses**

176

177 Total dissolved inorganic carbon (DIC) and NH<sub>4</sub><sup>+</sup> were measured by flow injection analysis  
178 with conductivity detection (Hall and Aller, 1992). Nitrate was measured  
179 spectrophotometrically (Parsons et al., 1984). Dissolved Fe<sup>2+</sup> was determined by colorimetric  
180 method with Ferrozine (Stookey, 1970). Dissolved Mn<sup>2+</sup> and Ca<sup>2+</sup> were analyzed in acidified  
181 pore water by inductively coupled plasma-atomic emission spectrometry (ICP-AES, Optima  
182 3300DV, Perkin-Elmer Co.) and flame atomic absorption spectrometer (SpectrAA 220/FS,  
183 Varian), respectively (Thamdrup and Canfield, 1996). Dissolved sulfide was determined by  
184 the methylene blue method (Cline, 1969). Sulfate concentrations were measured using ion  
185 chromatography (Metrohm 761). The detection limit of H<sub>2</sub>S, Ca<sup>2+</sup>, Mn<sup>2+</sup> and Fe<sup>2+</sup> was 3 µM,  
186 1.8 µM, 3 µM and 1 µM, respectively. Reproducibility of DIC and NH<sub>4</sub><sup>+</sup> was better than 10%.  
187 Precision of NO<sub>3</sub><sup>-</sup> was 1 – 2%.

188

## 189 **2.5 Solid-phase analyses**

190

191 Total oxalate-extractable Fe [Fe(II) + Fe(III)] was extracted from air-dried sediment in a 0.2  
192 M oxalic acid solution (pH 3) for 4 h (Thamdrup and Canfield, 1996), and Fe(II) was  
193 extracted from frozen sediment in anoxic oxalate (Phillips and Lovley, 1987). The total  
194 oxalate-extractable Fe and Fe(II), hereafter total Fe<sub>(oxal)</sub> and Fe(II)<sub>(oxal)</sub>, were determined as  
195 described for the pore-water analysis of Fe<sup>2+</sup>. Oxalate-extractable Fe(III), hereafter

196 Fe(III)<sub>(oxal)</sub>, was defined as the difference between total Fe<sub>(oxal)</sub> and Fe(II)<sub>(oxal)</sub>. This fraction  
197 represents poorly crystalline Fe(III) oxides. Particulate Mn, hereafter Mn<sub>(DCA)</sub> was extracted  
198 with dithionite-citrate-acetic acid (DCA; pH 4.8) for 4 h from air-dried sediment and was  
199 determined by inductively coupled plasma-atomic emission spectrometry (ICP-AES, Optima  
200 3300DV, Perkin-Elmer Co). The DCA extraction aims at dissolving free Mn oxides and  
201 authigenic Mn(II) phases. The reproducibility of the measurements was better than 10% and  
202 the detection limits was 3 μM for Mn and 1 μM for Fe. For the determination of total reduced  
203 sulfur (TRS) that includes acid volatile sulfide (AVS = FeS + H<sub>2</sub>S and small amounts of other  
204 metal sulfides, see Rickard and Morse, 2005; Luther, 2005) and chromium-reducible sulfur  
205 (CRS = S<sup>0</sup> + FeS<sub>2</sub>), sediment samples were fixed with Zn acetate, and sulfide was determined  
206 according to the method of Cline (1969) after a two-step distillation with cold 12 M HCl and  
207 boiling 0.5 M Cr<sup>2+</sup> solution (Fossing and Jørgensen, 1989). The contents of particulate  
208 organic carbon (POC) and nitrogen (PON) in the surface sediment were analyzed using a  
209 CHN analyzer (CE Instrument, EA 1110) after removing CaCO<sub>3</sub> using 12 M HCl.

210

## 211 **2.6 Oxygen micro-profiles**

212

213 Oxygen profiles were measured at 50 μm resolution using Clark-type microelectrodes  
214 (Unisense, OX-50) while stirring the overlying water. Microelectrodes were calibrated  
215 between 100% air-saturated *in situ* bottom water and N<sub>2</sub> purged anoxic bottom water. Three  
216 profiles were measured at each site. The diffusive boundary layer (DBL) and sediment-water  
217 interface (SWI) were determined according to Jørgensen and Revsbech (1985). To estimate  
218 the volume-specific oxygen consumption rate, we used the PROFILE software (Berg et al.,  
219 1998).

220

## 221 **2.7 Rate measurements**

222

223 The diffusive oxygen uptake (DOU) was calculated from the calibrated oxygen microprofiles.

224

$$225 \text{DOU} = -D_o \Delta C / \Delta z, \quad (1)$$

226

227 where  $D_o$  ( $1.07 \times 10^{-9} \text{ m}^2 \text{ s}^{-1}$  at M1 and  $1.03 \times 10^{-9} \text{ m}^2 \text{ s}^{-1}$  at D3) is the temperature-corrected  
228 molecular diffusion coefficient estimated from Schulz (2006), and  $C$  is the oxygen

229 concentration at depth z within the diffusive boundary layer (DBL) (Jørgensen and Revsbech,  
230 1985).

231 The volume-specific O<sub>2</sub> consumption rates exhibited a bimodal depth distribution (see  
232 results section 3.2) with activity peaks near the sediment-water interface and the oxic/anoxic  
233 interface, respectively. Thus, O<sub>2</sub> consumption rates by aerobic organotrophic respiration was  
234 defined as the O<sub>2</sub> consumption rate near the sediment-water interface, whereas the oxygen  
235 consumption at the oxic-anoxic interface was assigned to re-oxidation of reduced inorganic  
236 compounds (Rasmussen and Jørgensen, 1992; Canfield et al., 2005).

237 Total anaerobic C<sub>org</sub> mineralization rates were determined by linear regression of the  
238 accumulation of total DIC with time during the anoxic bag incubations (Fig. 3) after  
239 correcting for CaCO<sub>3</sub> precipitation (Thamdrup et al., 2000). Briefly, CaCO<sub>3</sub> precipitation was  
240 calculated from decreasing dissolved Ca<sup>2+</sup> concentration during the anoxic bag incubation:

241

$$242 \Delta\text{CaCO}_3 = \Delta[\text{Ca}^{2+}]_{\text{sol}} \times (1 + K_{\text{Ca}}), \quad (2)$$

243

244 where,  $K_{\text{Ca}}$  is the adsorption constant for Ca<sup>2+</sup> ( $K_{\text{Ca}} = 1.6$ ) (Li and Gregory, 1974). Then rate  
245 of DIC production rate corrected for CaCO<sub>3</sub> precipitation was calculated as:

246

$$247 \text{DIC production} = \text{DIC accumulation} + \text{CaCO}_3 \text{ precipitation} \quad (3)$$

248

249 Fe(III) reduction rates were determined by linear regression of the increase in solid-phase  
250 Fe(II)<sub>(oxal)</sub> content with time during anoxic bag incubations. The dissimilatory microbial Fe(III)  
251 reduction rate was derived by subtracting abiotic Fe reduction coupled to the oxidation of  
252 sulfide produced by sulfate reduction (Gribsholt et al. 2003):

253

$$254 \text{Dissimilatory microbial Fe(III) Red} = \text{Total Fe(III) Red} - \text{Abiotic Fe(III) Red} \quad (4)$$

255

256 assuming that abiotic Fe reduction coupled to H<sub>2</sub>S oxidation occurred at a stoichiometry of 2  
257 Fe(III) per 3 H<sub>2</sub>S (Pyzik and Sommer, 1981; Melton et al., 2014):

258



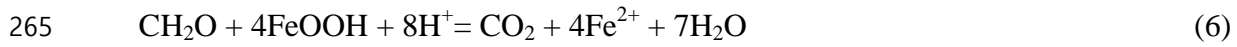
260

261 Finally, to estimate the C<sub>org</sub> oxidation by microbial Fe reduction, the 4:1 stoichiometry of



262 iron reduction coupled to  $C_{org}$  oxidation was used from the stoichiometric equation (Canfield  
263 et al., 1993a):

264



266

267 Mn reduction rates were determined from linear regression of the production of dissolved  
268  $\text{Mn}^{2+}$  with time during the anoxic bag incubations. Similar to previous studies (e.g., Canfield  
269 et al., 1993a, 1993b; Thamdrup and Dalsgaard, 2000), we assumed that accumulating  
270 dissolved Mn was  $\text{Mn}^{2+}$ . This ignores a potential contribution from  $\text{Mn}^{3+}$ , which in some  
271 cases can constitute a substantial fraction of the dissolved Mn pool at the upper boundary of  
272 the zone with soluble Mn accumulation in marine sediments (Madison et al., 2013). Further  
273 studies of the dynamics of soluble  $\text{Mn}^{3+}$  are required to evaluate its potential importance in  
274 anoxic incubations. Such studies pending, we find justification for our assumption in the  
275 good agreement observed in the previous studies between Mn reduction rates calculated  
276 based on the assumption that soluble Mn is  $\text{Mn}^{2+}$  (Eq. 7) and independent estimates of rates  
277 of carbon mineralization through dissimilatory Mn reduction based on DIC or  $\text{NH}_4^+$   
278 accumulation. Due to strong adsorption of  $\text{Mn}^{2+}$  to Mn oxide surfaces (Canfield et al., 1993b),  
279 the Mn reduction rates were estimated after compensating for the adsorption effect of  $\text{Mn}^{2+}$  to  
280 Mn-oxides according to Thamdrup and Dalsgaard (2000):

281

$$282 \quad \text{Mn reduction rate} = \text{Mn}^{2+} \text{ accumulation rate} \times (1 + K_{\text{Mn}}^{*2+} \times (1 - \Phi) \times \Phi^{-1} \times \delta_s) \quad (7)$$

283

284 where,  $\Phi$  = porosity

285  $\delta_s$  = density of sediment

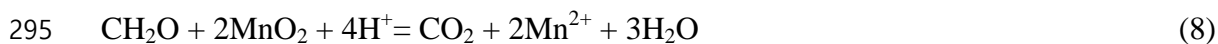
$$286 \quad K_{\text{Mn}}^{*2+} = 4.8 + 0.14 \times [\text{Mn(IV)}] \text{ (ml g}^{-1}\text{)}$$

$$287 \quad [\text{Mn(IV)}] = \text{the content of Mn(IV) (}\mu\text{mol g}^{-1}\text{)}$$

288

289 We here assume that extracted  $\text{Mn}_{(\text{DCA})}$  represents Mn(IV) as observed in surface  
290 sediments of another Mn-rich site (Canfield et al., 1993b, Thamdrup and Dalsgaard, 2000).  
291 Small levels of  $\text{Mn}_{(\text{DCA})}$  remaining at depth further suggest that little Mn(II) accumulates in  
292 the solid phase (*see* Results).  $C_{org}$  oxidation by dissimilatory Mn(IV) reduction was  
293 calculated from the stoichiometric equation (Canfield et al., 1993a):

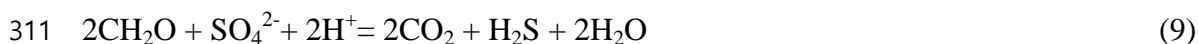
294



296

297 Sulfate reduction rates were determined using the radiotracer method of Jørgensen (1978).  
298 Sediment cores (35 cm long with 2.9 cm i.d.) were collected in triplicate, injected  
299 horizontally at 1-cm vertical interval with 5  $\mu\text{L}$  radiolabeled sulfate ( $^{35}\text{S}\text{-SO}_4^{2-}$ , 15 kBq  $\mu\text{L}^{-1}$ ,  
300 Amersham) diluted in sterilized NaCl solution (3.0 %), and incubated for 12 h at *in situ*  
301 temperature. At the end of the incubation, the sediment was sliced into sections, fixed in Zn  
302 acetate (20 %), and frozen at  $-25^\circ\text{C}$  until processed in the laboratory. The reduced  $^{35}\text{S}$  was  
303 recovered using distillation with a boiling acidic  $\text{Cr}^{2+}$  solution according to Fossing and  
304 Jørgensen (1989). Background radioactivity of  $^{35}\text{S}$  was  $32.4 \pm 3.7$  cpm  $\text{cm}^{-3}$  ( $n=10$ ) at site D3  
305 and  $87.5 \pm 38.7$  cpm  $\text{cm}^{-3}$  ( $n=10$ ) at site M1. Detection limits of the SRR, estimated from the  
306 double standard deviation of the blank value (i.e., 7.4 and 77.4 cpm) according to Fossing et  
307 al. (2000), ranged from 0.79 to 2.62  $\text{nmol cm}^{-3} \text{d}^{-1}$ . To elucidate the contribution of sulfate  
308 reduction in anaerobic carbon oxidation, the SRRs (Fig. 5B, 5G) were converted to carbon  
309 oxidation using a stoichiometric equation (Thamdrup and Canfield, 1996):

310



312

### 313 3 Results

314

#### 315 3.1 Pore-water and solid-phase constituents

316

317 The depth distributions of  $\text{NH}_4^+$ ,  $\text{NO}_3^-$ ,  $\text{Mn}^{2+}$  and  $\text{Fe}^{2+}$  in the pore-water as well as solid phase  
318 Mn, Fe and S for the two stations are shown in Fig. 2.  $\text{NH}_4^+$  concentrations at M1 increased  
319 steadily with depth (Fig. 2A) whereas at D3 it decreased down to 3 cm depth before it  
320 increased below (Fig. 2F). Highest concentrations of nitrate were measured at 0 to 1 cm  
321 sediment depth at the two stations and concentrations decreased below a background level ( $<$   
322  $2 \mu\text{M}$ ) below 1 cm at both M1 and D3 (Fig. 2A, 2F). Dissolved  $\text{Mn}^{2+}$  concentrations differed  
323 widely between the sites showing a maximum of  $56 \mu\text{M}$  between 0 and 3 cm depth and not  
324 exceeding  $10 \mu\text{M}$  below at M1 (Fig. 2B), whereas at D3 concentrations increased to a  
325 maximum of  $286 \mu\text{M}$  at 10 – 12 cm depth (Fig. 2G). Conversely, dissolved  $\text{Fe}^{2+}$

326 concentrations at M1 increased from 11  $\mu\text{M}$  at 0 – 0.5 cm to 32  $\mu\text{M}$  at 6 – 7 cm depth, and  
327 stayed constant below (Fig. 2C), whereas at D3, concentrations were uniformly low showing  
328 a slight increase to 12  $\mu\text{M}$  at 15 cm (Fig. 2F).

329 Extractable Mn ( $\text{Mn}_{(\text{DCA})}$ ) contents were low ( $< 3 \mu\text{mol cm}^{-3}$ ) in the upper 20 cm at the  
330 slope site (M1) (Fig. 2B), but up to 200  $\mu\text{mol cm}^{-3}$  in the upper 4 cm depth of the sediment at  
331 the center of the basin (D3), with a sharp decrease to near depletion ( $\sim 1 \mu\text{mol cm}^{-3}$ ) below 10  
332 cm (Fig. 2G). At the slope site (M1), contents of  $\text{Fe}(\text{III})_{(\text{oxal})}$  decreased slightly with  
333 increasing depth from 28  $\mu\text{mol cm}^{-3}$  near the surface to 13  $\mu\text{mol cm}^{-3}$  at 20 cm depth,  
334 mirroring an increase in  $\text{Fe}(\text{II})_{(\text{oxal})}$  (Fig. 2D). At the center of the basin (D3),  $\text{Fe}(\text{III})_{(\text{oxal})}$   
335 increased slightly from 67  $\mu\text{mol cm}^{-3}$  at 0 – 0.5 cm to 90  $\mu\text{mol cm}^{-3}$  at 4 – 6 cm depth, and  
336 decreased steeply below to 4.8  $\mu\text{mol cm}^{-3}$  at 12 – 14 cm depth (Fig. 2I). Of total  $\text{Fe}_{(\text{oxal})}$ ,  
337  $\text{Fe}(\text{III})_{(\text{oxal})}$  comprised  $> 98 \%$  at 0 – 2 cm and  $> 97 \%$  at 0 – 8 cm depth at M1 and D3,  
338 respectively. The fraction of  $\text{Fe}(\text{III})_{(\text{oxal})}$  in  $\text{Fe}_{(\text{oxal})}$  then decreased to 40 % at 10 – 12 cm depth  
339 at both sites. Acid volatile sulfur (AVS) exhibited a slight increase with depth at M1 from 0.8  
340  $\mu\text{mol cm}^{-3}$  at the surface to 7.2  $\mu\text{mol cm}^{-3}$  at 20 cm depth (Fig. 2E), but was not detected at  
341 D3 (Fig. 2J). Chromium reducible sulfur (CRS) contents at M1 increased rapidly with depth  
342 from 1.9  $\mu\text{mol cm}^{-3}$  at 0 – 0.5 cm to 21.8  $\mu\text{mol cm}^{-3}$  at 20 cm depth (Fig. 2D), whereas the  
343 CRS contents remained  $< 0.1 \mu\text{mol cm}^{-3}$  at D3 (Fig. 2J).

344

### 345 **3.2 $\text{O}_2$ microprofiles and diffusive oxygen uptake rate**

346

347 Oxygen penetrated less than 4 mm into the sediments (Fig. 3), and rates of diffusive oxygen  
348 uptake (DOU) were 7.1 and 6.0  $\text{mmol O}_2 \text{ m}^{-2} \text{ d}^{-1}$  at M1 and D3, respectively (Table 2).  
349 Oxygen consumption by aerobic respiration estimated from the  $\text{O}_2$  micro-profiles (area I and  
350 II in Fig. 3) was higher at the slope site M1 (4.0  $\text{mmol O}_2 \text{ m}^{-2} \text{ d}^{-1}$ ) than at the D3 in the center  
351 of the basin (2.5  $\text{mmol O}_2 \text{ m}^{-2} \text{ d}^{-1}$ ).  $\text{O}_2$  consumption by re-oxidation of reduced inorganic  
352 compounds indicated by increased activity at the oxic/anoxic interface (area III in Fig. 3)  
353 accounted for 43 % and 57 % of the DOU at M1 and D3, respectively. From the profiles of  
354 geochemical constituents (Fig. 2),  $\text{O}_2$  consumption was mainly attributed to the re-oxidation  
355 of sulfide and  $\text{Fe}^{2+}$  at M1 and of  $\text{Mn}^{2+}$  at D3.

356

### 357 **3.3 Anoxic bag incubations**

358

359 Changes in concentrations of DIC,  $\text{Ca}^{2+}$  and dissolved  $\text{Mn}^{2+}$  and solid  $\text{Fe(II)}_{(\text{oxal})}$  contents  
360 over time during anoxic bag incubations from sediment of 0 – 2, 2 – 4, 4 – 6 and 6 – 8 cm  
361 depth intervals are presented in Fig. 4. The DIC concentrations increased linearly over time  
362 during incubations of sediment in all bags from M1 and D3, except the bag from 6 – 8 cm at  
363 D3. The DIC accumulation rates were generally higher at the slope site (M1) than at the basin  
364 site (D3) (Table 4). The concentrations of  $\text{Ca}^{2+}$  decreased with time at all depth intervals of  
365 M1, whereas a decrease of  $\text{Ca}^{2+}$  was observed only for the 2 – 4 cm depth interval at D3. The  
366 decrease of  $\text{Ca}^{2+}$  indicates  $\text{CaCO}_3$  precipitation, which consequently underestimates DIC  
367 accumulation, especially at M1.

368 Coinciding with high solid  $\text{Mn}_{(\text{DCA})}$  contents (Fig. 2G), prominent  $\text{Mn}^{2+}$  accumulation  
369 appeared at 0 – 6 cm depth of D3, whereas no increase of  $\text{Mn}^{2+}$  was observed at M1 except a  
370 slight accumulation at 0 – 2 cm interval (Fig. 4). Solid  $\text{Fe(II)}_{(\text{oxal})}$  contents increased linearly  
371 with time at 0 – 4 cm depth of M1, whereas highest  $\text{Fe(II)}_{(\text{oxal})}$  accumulation was observed at  
372 4 – 6 cm depth at D3. An increase of  $\text{Fe(II)}_{(\text{oxal})}$  was not discernible in the Mn-oxide-rich  
373 surface sediment (0 – 2 cm) of D3.

374

### 375 **3.4 Sulfate reduction rates (SRR)**

376

377 At the slope site (M1), SRR increased from  $18 \text{ nmol cm}^{-3} \text{ d}^{-1}$  at the surface to  $97 - 103 \text{ nmol}$   
378  $\text{cm}^{-3} \text{ d}^{-1}$  at 1.5 – 2 cm depth, and decreased below to  $12.5 \text{ nmol cm}^{-3} \text{ d}^{-1}$  at 20 cm depth (Fig.  
379 5B). In contrast, SRR at the manganese oxide-rich basin site (D3) ranged from 1.7 to 8.7  
380  $\text{nmol cm}^{-3} \text{ d}^{-1}$ , and did not vary with depth. Depth integrated SRR down to 10 cm depth was  
381 10 times higher at M1 ( $4.3 \text{ mmol m}^{-2} \text{ d}^{-1}$ ) than at D3 ( $0.4 \text{ mmol m}^{-2} \text{ d}^{-1}$ ) (Table 3).

382

### 383 **3.5 DIC production rates**

384

385 Vertical profiles of the DIC production rate that were derived from the linear regression of  
386 the DIC production measured in anoxic bag incubation (Fig. 4) after correcting for  $\text{CaCO}_3$   
387 precipitation, are presented in Fig. 5C and 5H for M1 and D3, respectively. At M1, the DIC  
388 production rates decreased with depth from  $280 \text{ nmol cm}^{-3} \text{ d}^{-1}$  (0 – 2 cm depth) to  $69 \text{ nmol}$   
389  $\text{cm}^{-3} \text{ d}^{-1}$  (8 – 10 cm depth) (Fig. 5C), whereas the DIC production rates at D3 were relatively  
390 similar across the upper 6 cm ranging from 86 to  $136 \text{ nmol cm}^{-3} \text{ d}^{-1}$ , and decreased to 8 – 15  
391  $\text{nmol cm}^{-3} \text{ d}^{-1}$  at 6– 10 cm (Fig. 5H). The integrated DIC production rate within 10 cm depth

392 of the sediment was twice as high at M1 ( $14.0 \text{ mmol m}^{-2} \text{ d}^{-1}$ ) as at the D3 ( $7.2 \text{ mmol m}^{-2} \text{ d}^{-1}$ )  
393 (Table 4).

394

### 395 **3.6 Rates of Mn and Fe reduction**

396

397 The accumulation of  $\text{Mn}^{2+}$  presented evidence that manganese reduction was occurring in the  
398 surface sediment (0 – 6 cm) of D3 (Fig. 4). The manganese reduction rate (MnRR) derived  
399 from  $\text{Mn}^{2+}$  accumulation with correction for adsorption ranged from  $7.5 \text{ nmol cm}^{-3} \text{ d}^{-1}$  (0 – 2  
400 cm depth) to  $198 \text{ nmol cm}^{-3} \text{ d}^{-1}$  (2 – 4 cm depth) at D3 (Fig. 5I). In contrast, MnRR at M1  
401 was indiscernible except for low activity ( $2.2 \text{ nmol cm}^{-3} \text{ d}^{-1}$ ) at 0 – 2 cm depth (Fig. 5D).  
402 Depth integrated MnRR at D3 ( $8.21 \text{ mmol m}^{-2} \text{ d}^{-1}$ ) was 200 times higher than the MnRR at  
403 M1 ( $0.04 \text{ mmol m}^{-2} \text{ d}^{-1}$ ) (Table 3). The iron reduction rate (FeRR), derived from  $\text{Fe(II)}_{(\text{oxal})}$   
404 accumulation, at M1 was highest in the 0 – 2 cm interval ( $237 \text{ nmol cm}^{-3} \text{ d}^{-1}$ ), and then  
405 decreased with depth to  $38 \text{ nmol cm}^{-3} \text{ d}^{-1}$  at 8 – 10 cm depth (Fig. 5E). In contrast, Fe  
406 reduction was not detected in the surface sediment at D3, but increased to its maximum rate  
407 of  $240 \text{ nmol cm}^{-3} \text{ d}^{-1}$  at 4 – 6 cm depth. The FeRR then decreased with depth to  $12 \text{ nmol cm}^{-3}$   
408  $\text{d}^{-1}$  at 8 – 10 cm (Fig. 5J) where a few data points were adopted to derive the line of best-fit  
409 regression. Depth integrated total FeRR was slightly higher at M1 ( $11.4 \text{ mmol m}^{-2} \text{ d}^{-1}$ ) than at  
410 D3 ( $7.53 \text{ mmol m}^{-2} \text{ d}^{-1}$ ) (Table 3). The ratio of microbial Fe reduction,  $\text{Fe Red}_{(\text{microbial})}$ , to  
411 abiotic Fe reduction coupled to sulfide oxidation,  $\text{Fe Red}_{(\text{abiotic})}$ , ranged from 1.14 (8 – 10 cm  
412 at M1) to 52.3 (2 – 4 cm at D3), which indicated that the Fe reduction at Mn- and Fe oxides  
413 rich basin site was mostly a microbiologically mediated process (Table 3).

414

## 415 **4 Discussion**

416

### 417 **4.1 Partitioning of $\text{C}_{\text{org}}$ oxidation in accordance with the distribution of terminal** 418 **electron acceptors**

419

420 One of the most prominent features revealed from the vertical distributions of geochemical  
421 constituents at the basin site (D3) was that electron acceptors such as  $\text{O}_2$ , nitrate, Mn- and Fe  
422 oxides were systematically distributed with discrete zonation according to the order of  
423 decreasing energy yield for  $\text{C}_{\text{org}}$  oxidation (Fig. 5F). Such biogeochemical zones are not  
424 sharply separated in most aquatic sediments due to, e.g., sediment heterogeneity and mixing

425 resulting from bioirrigation, bioturbation, and bottom turbidity currents. The profiles of  
426 dissolved and solid phase geochemical constituents in the sediment provide indications as to  
427 specific diagenetic reactions prevailing (Froelich et al., 1979). However, reoxidation of  
428 reduced inorganic compounds often mask the primary reactions involved in carbon oxidation  
429 (Sørensen and Jørgensen, 1987; Hines et al., 1991). Together with the discrete geochemical  
430 zonation of the electron acceptors, the independently executed metabolic rate measurements  
431 (Fig. 5) allowed us to evaluate the relative contribution of each terminal electron-accepting  
432 pathway with sediment depth.

433 Previous experimental studies that have quantified pathways of anaerobic carbon  
434 oxidation in subtidal marine sediments have generally determined the contributions of Mn  
435 and Fe reduction indirectly from the difference between rates of DIC production and sulfate  
436 reduction converted to carbon equivalents (e.g., Canfield et al., 1993b; Thamdrup and  
437 Canfield, 1996; Vandieken et al., 2006). The inferred rates of Mn and Fe reduction were  
438 further supported by the depth distribution of metal oxides and patterns of  $\text{Mn}^{2+}$  and  $\text{Fe}^{2+}$   
439 accumulation in the pore water, but could not be verified because the accumulation of  
440 particulate Mn(II) and Fe(II) – which represents the overwhelming fraction of the reduced  
441 pools – was not quantified. Here, we combined the indirect approach with independent  
442 determination of Mn and Fe reduction rates. Thus, we obtained two separate estimates of  
443 anaerobic carbon oxidation rates; based on DIC production and on the sum of sulfate, Fe, and  
444 Mn reduction converted to carbon equivalents, respectively (Table 4). At M1, within the 0 –  
445 10 cm depth interval, the average ratio between total anaerobic  $C_{\text{org}}$  oxidation rate ( $10.7$   
446  $\text{mmol C m}^{-2} \text{d}^{-1}$ ) and the  $C_{\text{org}}$  oxidation from DIC production ( $14.0 \text{ mmol C m}^{-2} \text{d}^{-1}$ ) was 0.77  
447 (Table 4). Similarly, at D3, the average ratio between total anaerobic  $C_{\text{org}}$  oxidation ( $6.79$   
448  $\text{mmol m}^{-2} \text{d}^{-1}$ ) and anaerobic DIC production ( $7.22 \text{ mmol m}^{-2} \text{d}^{-1}$ ) was 0.94. There was a good  
449 agreement between the two estimates with a ratio of total anaerobic  $C_{\text{org}}$  oxidation by Mn +  
450 Fe + sulfate : DIC production for individual depth intervals of 0.8 – 1.2 (Table 4) with the  
451 exception at the 0 – 2 cm depth of slope site (M1) where the ratio was slightly lower, 0.66,  
452 possibly due to a contribution from the  $C_{\text{org}}$  oxidation by nitrate reduction. The similarity of  
453 the two estimates across all incubations spanning a range of redox conditions provides  
454 confidence in our approach for calculating dissimilatory Mn and Fe reduction rates.  
455 Specifically, the good agreement indicates that the underlying assumptions concerning Mn  
456 adsorption and reactions of Fe(III) and sulfide are valid as first-order approximations. The  
457 general agreement further supports the validity of previous determinations of dissimilatory

458 Mn and Fe reduction rates based on the difference between DIC production and  $\text{SO}_4^{2-}$   
459 reduction (Canfield et al., 1993a, 1993b; Thamdrup et al., 2000; Vandieken et al., 2006;  
460 Vandieken et al., 2014).

461 To elucidate the contribution of sulfate reduction in anaerobic carbon oxidation, the SRRs  
462 (Fig. 5B, 5G) were converted to carbon oxidation (Thamdrup and Canfield, 1996), and then  
463 compared to the DIC production rates from anoxic bag incubation (Fig. 5C, 5H). At the slope  
464 site (M1), the fraction of anaerobic  $\text{C}_{\text{org}}$  oxidation coupled to sulfate reduction increased with  
465 depth from 48 % at 0 – 2 cm, to 80 % at 8 – 10 cm (Table 4). Thus, the excess  $\text{C}_{\text{org}}$  oxidation  
466 in the upper layers should be coupled to other electron accepting processes. Indeed, the  $\text{C}_{\text{org}}$   
467 oxidation by Fe reduction ( $0.96 \text{ mmol m}^{-2} \text{ d}^{-1}$ ) accounted for most of the remaining anaerobic  
468  $\text{C}_{\text{org}}$  oxidation (12 – 18 % of DIC production) at 0 – 8 cm depth, consistent with the  
469 distribution of Fe(III) decreasing from  $> 25 \mu\text{mol cm}^{-3}$  near the surface (Fig. 6, Table 4). Mn  
470 reduction was of minor importance at M1 because of the low content of Mn oxide ( $< 3 \mu\text{mol}$   
471  $\text{cm}^{-3}$ ). Carbon oxidation coupled to aerobic respiration was estimated to  $3.1 \text{ mmol m}^{-2} \text{ d}^{-1}$   
472 corresponding to 18 % of the total aerobic + anaerobic oxidation, while the contributions of  
473 Fe and sulfate reduction to this total were 12 % and 50 %, respectively (Table 4). As  
474 mentioned above, nitrate reduction/denitrification may contribute part of the unexplained 19%  
475 of carbon oxidation, but most of this imbalance likely reflects the combined uncertainties in  
476 the estimates of the individual pathways. Additionally, our partitioning of carbon oxidation  
477 pathways could be biased towards the anaerobic electron acceptors due to the use of the  
478 diffusive oxygen uptake (DOU) rather than total oxygen uptake (TOU), which will exceed  
479 DOU if bioirrigation is active (Glud 2008). Bioirrigation was not determined at our sites, but  
480 the pore water profiles show no indication of strong irrigation (Fig. 2). An average  
481 DOU/TOU ratio of  $\sim 0.6$  has been reported for sediments at 1.5 – 2.5 km depth (Glud 2008).  
482 Using this ratio, and assuming that TOU is partitioned similarly as DOU between aerobic  
483 carbon oxidation and reoxidation, aerobic carbon oxidation would account for 25 %, while Fe  
484 and sulfate reduction would account for 11 % and 46 % of carbon oxidation, respectively.  
485 This, the potential bias from using DOU is not expected to affect the ranking of electron  
486 acceptors by quantitative importance ( $\text{SO}_4^{2-} > \text{O}_2 > \text{Fe(III)}$ ), and, as discussed further below,  
487 the partitioning of  $\text{C}_{\text{org}}$  oxidation at M1 falls within the range previously reported for  
488 continental margin sediments.

489 In contrast to M1,  $\text{C}_{\text{org}}$  oxidation by sulfate reduction at the basin site (D3) accounted for  
490 only a small fraction ( $< 11 \%$ ) of anaerobic  $\text{C}_{\text{org}}$  oxidation at 0 – 6 cm interval and it only

491 dominated carbon oxidation at 8 – 10 cm (Fig. 5H, Table 4). Oxygen and  $\text{NO}_3^-$  were depleted  
492 within 3.6 mm and 1 cm depth of the sediment surface, respectively (Fig. 5F), while Mn and  
493 Fe(III) oxides were abundant at 0 – 4 cm and 0– 6 cm, respectively. Consistent with the  
494 abundance of electron acceptors, high rates of Mn and Fe reduction (Fig. 5I and 5J) implied  
495 Mn and Fe reduction as the most significant  $\text{C}_{\text{org}}$  oxidation pathways to 6 cm depth. At 0 – 2  
496 cm depth,  $\text{C}_{\text{org}}$  oxidation by aerobic respiration and Mn reduction accounted for 53 % and 43 %  
497 of total  $\text{C}_{\text{org}}$  oxidation, respectively (Fig. 6). At 2 – 4 cm, Mn reduction accounted for 73 % of  
498 total  $\text{C}_{\text{org}}$  oxidation and 92 % of anaerobic  $\text{C}_{\text{org}}$  oxidation (Table 4, Fig. 6). Its importance  
499 decreased to 22 % at 4 – 6 cm due to lower Mn contents, while microbial Fe(III) reduction  
500 here contributed 51 %, and the partitioning of sulfate reduction increased to 11 % (Fig. 6).  
501 Consequently, the relative distribution of each  $\text{C}_{\text{org}}$  oxidation pathway with depth at D3 (Fig. 6)  
502 matched well with the depth distribution of the respective electron acceptors (Fig. 5F).  
503 Overall, within the 10 cm depth sediment interval, Mn and Fe reduction were the dominant  
504  $\text{C}_{\text{org}}$  oxidation pathways comprising 45 % and 20 % of total carbon oxidation, respectively, at  
505 the Mn and Fe oxide-rich site in the center of the UB (Table 4). Correction for a potential  
506 underestimation of TOU, as discussed for M1, would reduce the contributions of Mn and Fe  
507 reduction slightly to 41 % and 18 %, respectively.

508 Despite the high Fe oxide content at 0 – 4 cm at D3 (Fig. 5F), no solid  $\text{Fe(II)}_{(\text{oxal})}$   
509 accumulation was observed at this depth range (Fig. 6). This indicates that Fe(III) reduction  
510 may not occur under these Mn-oxide rich conditions. Indeed, using a combination of 16S  
511 rRNA-stable isotope probing and geochemical analysis in three manganese oxides-rich  
512 sediments including the UB, Vandieken et al. (2012) identified bacteria related to *Colwellia*,  
513 *Oceanospillaceae* and *Arcobacter* as acetate-oxidizing bacteria that potentially reduce  
514 manganese, whereas no known iron reducers were detected in the Mn-rich sediment.  
515 Similarly, Thamdrup et al. (2000), in Mn oxide- rich Black Sea sediment, found that the  
516 abundance of viable Fe-reducing bacteria in most probable number counts was low in  
517 comparison to Mn reducers and the addition of ferrihydrite did not stimulate Fe reduction,  
518 which implied that Fe reduction should be outcompeted by the Mn reduction process.

519 Nonetheless, Mn reduction estimated from the increase of  $\text{Mn}^{2+}$  at 0 – 4 cm interval at D3  
520 (Fig. 6) could be due to oxidation of  $\text{Fe}^{2+}$  or sulfide.  $\text{Fe}^{2+}$  may readily react with Mn oxides  
521 (Myers and Nealson, 1988; Lovley and Phillips, 1988) by the reaction  $2\text{Fe}^{2+} + \text{MnO}_2 + 4\text{H}_2\text{O}$   
522  $= \text{Mn}^{2+} + 2\text{Fe(OH)}_3 + 2\text{H}^+$ . However, in the Mn oxide-rich sediment of the Skagerrak,  
523 Canfield et al. (1993b) revealed that the addition of Ferrozine, a strong complexation agent



524 for  $\text{Fe}^{2+}$ , had no inhibitory effect on the  $\text{Mn}^{2+}$  liberation, indicating that the chemical reaction  
525 of  $\text{MnO}_2$  with  $\text{Fe}^{2+}$  generated by Fe reduction was not responsible for the accumulation of  
526  $\text{Mn}^{2+}$ . As manganese reduction is thermodynamically more favorable than iron and sulfate  
527 reduction, the  $\text{Mn}^{2+}$  liberation (Fig. 3) likely resulted from dissimilatory Mn reduction.

528 Despite the anoxic conditions and nitrate depletion during the bag incubation, Mn  
529 reduction rates at 0 – 2 cm depth (Fig. 5I) based on  $\text{Mn}^{2+}$  accumulation were substantially  
530 lower than the rates inferred from DIC accumulation (Fig. 5H). A similar discrepancy was  
531 previously observed for the uppermost part of the Mn reduction zone (Thamdrup et al., 2000),  
532 and is likely explained by particularly strong sorption of  $\text{Mn}^{2+}$  to fresh Mn oxide surfaces,  
533 which is not included in the adsorption coefficient used here. Low  $\text{Mn}^{2+}$  together with the  
534 rapid decrease of nitrate at 0-2 cm depth at D3 (Fig. 2F, 2G) also suggested that dissolved  
535 reduced manganese might act as a reducing agent for nitrate as it was suggested by Aller et al.  
536 (1998) in the Panama Basin and Mogollón et al. (2016) in the deep-sea sediment of the  
537 Clarion-Clerton fracture zone in the northeast equatorial Pacific.

538 Previous estimation of denitrification in 0 – 2 cm depth of the UB ranged from 0.01 to  
539  $0.17 \text{ mmol N m}^{-2} \text{ d}^{-1}$  (Lee, 2009), which is equivalent to a  $\text{C}_{\text{org}}$  oxidation of 0.013– 0.213  
540  $\text{mmol C m}^{-2} \text{ d}^{-1}$  using the stoichiometric equation of  $4\text{H}^+ + 5\text{CH}_2\text{O} + 4\text{NO}_3^- = 5\text{CO}_2 + 2\text{N}_2 +$   
541  $7\text{H}_2\text{O}$ . Based on the average, the contribution of carbon oxidation by denitrification ( $0.11$   
542  $\text{mmol C m}^{-2} \text{ d}^{-1}$ ) should be minor at the basin site ( $\leq 3\%$  of total  $\text{C}_{\text{org}}$  oxidation at 0 – 2 cm;  
543  $\sim 1\%$  of integrated  $\text{C}_{\text{org}}$  oxidation). This is consistent with the general consensus that  $\text{C}_{\text{org}}$   
544 oxidation by denitrification is of little importance in most marine sediments (Sørensen et al.,  
545 1979; Canfield et al., 1993a; Trimmer and Engström, 2011). Denitrification may be even  
546 further suppressed in Mn-rich sediments due to competitive inhibition from Mn reduction  
547 (Trimmer et al., 2013).

548

#### 549 **4.2 $\text{C}_{\text{org}}$ oxidation dominated by manganese reduction in the UB**

550

551 Microbial Fe reduction has been quantified directly in sediments of various coastal oceans  
552 (Gribsholt et al., 2003; Kostka et al., 2002a, 2002b; Hyun et al., 2007, 2009b) and indirectly  
553 in deeper continental margins (Thamdrup and Canfield, 1996; Jensen et al., 2003; Kostka et  
554 al., 1999). Earlier estimation from 16 different continental margin sediments indicated that  
555 Fe(III) reduction contributed 22 % on average to anaerobic carbon oxidation (Thamdrup,  
556 2000). Thus, the contributions from Fe(III) reduction of 12 % and 20 % of anaerobic  $\text{C}_{\text{org}}$

557 oxidation on the slope (M1) and in the basin (D3) of the UB (Table 4) fall in the range of the  
558 previous indirect estimates.

559 Unlike Fe reduction, direct estimation of manganese reduction rates is not easy, mainly  
560 because of the restriction of the process to a thin surface layer (Sundby and Silverberg, 1985),  
561 the rapid reduction of manganese oxides with  $\text{H}_2\text{S}$  and  $\text{Fe}^{2+}$  (Postma, 1985; Burdige and  
562 Nealson, 1986; Kostka et al., 1995; Lovley and Phillips, 1988), and the adsorption of  $\text{Mn}^{2+}$  to  
563 Mn oxide surface (Canfield et al., 1993b). For that reason, only two studies, from the  
564 Skagerrak and Black Sea, are available for direct comparison on the partitioning of Mn  
565 reduction. The process has also been indicated to be of importance in the Panama Basin based  
566 on diagenetic modeling (Aller, 1990) and at some Arctic shelf sites where it was however not  
567 quantified separately from Fe reduction (Vandieken et al., 2006, Nickel et al., 2008). Mn  
568 reduction was responsible for over 90 % of total  $\text{C}_{\text{org}}$  oxidation at 600 m depth in the  
569 Skagerrak (Canfield et al., 1993b), and accounted for 13 – 45 % of anaerobic  $\text{C}_{\text{org}}$  oxidation  
570 in the Black Sea shelf sites at 60 – 130 m of water depth (Thamdrup et al., 2000). To our  
571 knowledge, this report of  $\text{C}_{\text{org}}$  oxidation dominated by Mn reduction comprising 45 % of total  
572  $\text{C}_{\text{org}}$  oxidation and 57 % of anaerobic  $\text{C}_{\text{org}}$  respiration in the center of the UB (Table 4)  
573 represents the first from deep-offshore basin of the eastern Asian marginal seas.

574 The difference in partitioning of Mn reduction in  $\text{C}_{\text{org}}$  oxidation between the UB, Black  
575 Sea and Skagerrak reflects the close relationship between Mn oxide content in the sediment  
576 and Mn reduction (Thamdrup et al., 2000). From the vertical distribution of electron  
577 acceptors (Fig. 5J) and contribution of each  $\text{C}_{\text{org}}$  oxidation pathway with depth (Fig. 6), it is  
578 apparent that the availability of Mn(IV) largely controls the relative contribution to C  
579 oxidation. In the Skagerrak, the Mn oxides are abundant in high content down to 10 cm depth  
580 (Canfield et al., 1993b), whereas Mn oxides in the Black Sea and the Ulleung Basin were  
581 enriched only down to 2 cm and 4 cm, respectively (Thamdrup et al., 2000, Fig. 2). Using the  
582 available data set for the three marine sediments, we further plotted the relative contribution  
583 of manganese reduction to anaerobic carbon oxidation as a function of Mn-oxides content to  
584 expand data from Thamdrup et al., 2000 (Fig. 7). The plot indicates saturation kinetics with a  
585 close correlation between Mn oxide content and the importance of Mn reduction at low  
586 contents. Curve-fitting yields a concentration of  $\text{MnO}_2$  at 50% of contribution of manganese  
587 reduction to total  $\text{C}_{\text{org}}$  oxidation ( $K_s$ ) of  $8.6 \mu\text{mol cm}^{-3}$  similar to the approx.  $10 \mu\text{mol cm}^{-3}$   
588 suggested before (Thamdrup et al., 2000). This indicates that Mn reduction can be a dominant  
589  $\text{C}_{\text{org}}$  oxidation process even at low contents of Mn oxides compared to those found at UB.

590 Manganese enrichments of this magnitude have been reported for several locations on the  
591 continental margins and in deep basins (Murray et al., 1984; Gingele and Kasten, 1994;  
592 Gobeil et al., 1997; Haese et al., 2000; Mouret et al., 2009; Magen et al., 2011; Macdonald  
593 and Gobeil, 2012; Mewes et al., 2014) in addition to the relatively few places where  
594 dissimilatory Mn reduction was already indicated to be of importance, as discussed above.  
595 Thus, the process may be of more widespread significance, particularly in deep basin settings  
596 such as UB that allow geochemical focusing of manganese.

597

### 598 **4.3 Source of high Mn oxide content**

599

600 The strong enrichment of Mn in the UB surface sediment is primarily of diagenetic origin as  
601 indicated by similar Mn contents at depth in the sediment at D3 ( $0.95 - 3.02 \mu\text{mol cm}^{-3}$ )  
602 compared to M1 ( $0.36 - 3.74 \mu\text{mol cm}^{-3}$ ) (Fig. 2) combined with higher sediment  
603 accumulation rates at the slope ( $0.15 - 0.3 \text{ cm y}^{-1}$ ) than in the basin ( $0.07 \text{ cm y}^{-1}$ ; Cha et al.,  
604 2005). Thus, the burial flux of Mn, and thereby the net input assuming steady state deposition,  
605 is higher at M1 than at D3. Furthermore, Mn is likely subject to geochemical focusing in the  
606 basin as Mn depositing at shallower depths is reductively mobilized and incompletely  
607 oxidized in the thin oxic surface layer, resulting in release to the water column and net down-  
608 slope transport, as inferred in other ventilated basins (Sundby and Silverberg, 1985; Canfield  
609 et al., 1993b; Schaller and Wehrli, 1997). A diagenetic source of Mn enrichment was also  
610 concluded in previous studies (Yin et al., 1989; Cha et al., 2007; Choi et al., 2009). The Mn  
611 remaining and being buried at M1 likely represents unreactive detrital forms to a larger extent  
612 than at D3 (Cha et al., 2007). Adopting the sediment accumulation rate of  $0.07 \text{ cm y}^{-1}$  in the  
613 UB determined at a station 50 km from D3 (Cha et al., 2005), the average  $\text{Mn}_{(\text{DCA})}$  content of  
614  $1.1 \mu\text{mol cm}^{-3}$  at 10 – 20 cm depth (Fig. 2G) corresponds to a flux for permanent burial of  
615  $0.002 \text{ mmol m}^{-2} \text{ d}^{-1}$  or just 0.03 % of the Mn reduction rate (Table 3), i.e., an Mn atom is  
616 recycled 3800 times before it finally gets buried – first by stripping from the particles that  
617 settle to the seafloor and subsequently, over and over, by reductive dissolution of the Mn  
618 oxides that form by reoxidation in the oxic surface layer (or, potentially, in the nitrate zone;  
619 Aller et al., 1998; Mogollón et al., 2016). This is a much more extensive recycling than found  
620 in the Mn sediment of Skagerrak (130 – 260 times; Canfield et al., 1993b). The difference  
621 results mainly from a much higher burial flux of Mn (as authigenic Mn(II)) in the Skagerrak  
622 ( $\sim 40 \mu\text{mol cm}^{-3}$ ; Canfield et al., 1993b). The reason that little, if any, authigenic Mn(II) is

623 buried in the UB is not clear.

624 As noted in previous studies (Aller, 1990; Canfield et al., 1993b), high contributions of  
625 Mn and Fe reduction to carbon oxidation in off-shore sediments requires physical mixing,  
626 which typically occurs through bioturbation. This is also the case for the UB, where the burial  
627 flux from the oxic surface layer into the Mn reduction zone corresponded to  $0.4 \text{ mmol m}^{-2} \text{ d}^{-1}$   
628 or 5 % of the Mn reduction rate ( $213 \text{ } \mu\text{mol cm}^{-3} \times 0.07 \text{ cm y}^{-1}$ ). Bioturbation has previously  
629 been inferred, but not quantified, from  $^{210}\text{Pb}$  profiles in the UB (Cha, 2002), and thin  
630 polychaete worms were observed during our sampling. Assuming bioturbation to be a  
631 diffusive process, we estimate, in a similar manner as in the previous studies and based on the  
632 average gradient in  $\text{Mn}_{(\text{DCA})}$  from 0.5 – 1 to 7 – 8 cm, that the Mn reduction rate would be  
633 supported at a biodiffusion coefficient of  $9.5 \text{ cm}^2 \text{ y}^{-1}$ . This value is 3.6 times lower than the  
634 coefficient estimated for the Skagerrak (Canfield et al., 1993b) and consistent with estimates  
635 for other sediments with similar deposition rates (Boudreau, 1994). Thus, it is realistic that  
636 bioturbation drives Mn cycling in the UB.

637

#### 638 **4.4 The UB as a biogeochemical hotspot**

639

640 The SRRs measured in this study ( $0.43 - 4.29 \text{ mmol m}^{-2} \text{ d}^{-1}$ ) are higher than those measured  
641 in productive systems such as the Benguela upwelling system in the Southeast Atlantic  
642 (Ferdelman et al., 1999; Fossing et al., 2000), and even comparable to those reported at the  
643 continental slope of the Chilean upwelling system ( $2.7 - 4.8 \text{ mmol m}^{-2} \text{ d}^{-1}$ ) (Thamdrup and  
644 Canfield, 1996) at a similar depth range of 1000 – 2500 m. The total anaerobic DIC  
645 production rates at the slope ( $14.0 \text{ mmol m}^{-2} \text{ d}^{-1}$ ) and basin site ( $7.2 \text{ mmol m}^{-2} \text{ d}^{-1}$ ) were also  
646 comparable to those measured at the same depth range of a Chilean upwelling site ( $9.2 - 11.6$   
647  $\text{mmol m}^{-2} \text{ d}^{-1}$ ) (Thamdrup and Canfield, 1996). Since rates of benthic carbon oxidation are  
648 largely controlled by the supply of organic carbon (Canfield et al., 2005), a high organic  
649 carbon flux reflected in the high organic carbon content ( $> 2.5\%$ , dry wt.) in the sediment of  
650 the UB (Table 1) is likely to explain the high metabolic activities. A similar high organic  
651 carbon content as in the UB is rarely found in deep-sea sediment underlying oxic bottom  
652 water at depths exceeding 2000 m, except for a Chilean upwelling site (Lee et al., 2008). This  
653 high organic carbon content in the UB is mainly associated with the combination of enhanced  
654 biological production resulting from the formation of coastal upwelling (Hyun et al., 2009a),  
655 occurrence of an intrathermocline eddy resulting in the extraordinary subsurface chlorophyll-

656 a maximum (Kim et al., 2012), high organic C accumulation rates exceeding  $2 \text{ g C m}^{-2} \text{ yr}^{-1}$   
657 (Lee et al., 2008), and high export production (Kim et al., 2009). In addition to the large  
658 vertical sinking flux, the lateral transport of the organic matter along the highly productive  
659 southeastern slope of the UB also contributes to the high organic carbon content (Lee et al.,  
660 2015). Consequently, high benthic mineralization resulting from the high organic content in  
661 the sediment implied that the UB is a biogeochemical hotspot where significant turnover of  
662 organic matter and nutrient regeneration occur.

663 The East Seas often called as “a miniature ocean” because of the independent  
664 thermohaline convection system that is driven by the high density surface water sinking (Kim  
665 et al., 2001) in a manner similar to that of the Great Ocean Conveyor Belt (Broecker, 1991).  
666 The turnover time (ca. 100 – 300 years) of the thermohaline circulation is shorter than that of  
667 the global conveyor belt of 1000 – 2000 years (Broecker and Peng, 1982). Because of the  
668 shorter time-scale, together with the relatively small volume, the East Sea is expected to be  
669 much more sensitive to global environmental changes (such as global warming) compared  
670 with the open oceans. In this regard, the East Sea has been considered as a natural laboratory  
671 that provides a useful field for large-scale oceanographic experiments to predict the response  
672 of oceans associated with long-term climatic/oceanographic changes (Kim et al., 2001). Over  
673 the last two decades (1982 – 2006), a rapid increase of sea surface temperature (SST) of  
674  $1.09 \text{ }^{\circ}\text{C}$  has been recorded in the East Sea, which is the fourth highest among the 18 large  
675 marine ecosystems in the world ocean (Belkin, 2009). Increased SST reduces the solubility of  
676  $\text{O}_2$  in the surface mixed layer and enhances stratification, which ultimately affects biological  
677 production in the water column and suppresses transport of  $\text{O}_2$ -rich surface water into the  
678 deep bottom. Indeed, recent oceanographic observations revealed that the gradual  
679 deoxygenation and warming of the bottom water of the East Sea over the last 30 years have  
680 resulted in an  $\sim 10 \%$  decrease in dissolved oxygen and  $\sim 0.04 \text{ }^{\circ}\text{C}$  increase in potential  
681 temperature, which suggested a weakening of the deep convection system (Kim et al., 2001;  
682 Gamo et al., 2011). Benthic metabolism and respiratory  $\text{C}_{\text{org}}$  oxidation coupled to various  
683 TEAP in the sediments are largely controlled by the combination of  $\text{O}_2$  content, temperature  
684 and biological production overlying water column (Canfield et al., 2005). It is thus important  
685 to monitor any changes in the rates and partitioning of  $\text{C}_{\text{org}}$  oxidation to better understand and  
686 predict the variations of biogeochemical cycles of carbon, nutrients and metals potentially  
687 associated with long-term climatic changes in the UB, the biogeochemical hotspot of the East  
688 Sea.

689

## 690 **5. Conclusions**

691

692 Surface sediments of the Ulleung Basin (UB) in the far east Eurasian continent are  
693 characterized by a high organic carbon content ( $> 2.5\%$ , dry wt.), high contents Fe oxides  
694 (up to  $100\ \mu\text{mol cm}^{-3}$ ), and very high contents of Mn oxides ( $> 200\ \mu\text{mol cm}^{-3}$ ). We show that  
695 microbial Mn and Fe reduction are the dominant  $C_{\text{org}}$  oxidation pathways, comprising 45 %  
696 and 20 % of total  $C_{\text{org}}$  oxidation, respectively. The high Mn content results from highly  
697 efficient recycling through reoxidation with very low permant burial of authigenic Mn(II)  
698 phases. The basin topography may ensure that any  $\text{Mn}^{2+}$  escaping to the overlying water  
699 returns to the sediment after reprecipitation. The relative importance of Mn reduction to  $C_{\text{org}}$   
700 oxidation displays saturation kinetics with respect to Mn oxide content with a low half-  
701 saturation value ( $8.6\ \mu\text{mol cm}^{-3}$ ), which further implies that Mn reduction can be a dominant  
702  $C_{\text{org}}$  oxidation process in sediments with lower  $\text{MnO}_2$  content, and thereby that the process  
703 might be more important in continental margin and deep basin sediments than previously  
704 thought. Vertical distributions of the major terminal electron acceptors such as  $\text{O}_2$ , nitrate,  
705 Mn- and Fe oxides were systematically zoned with discrete sequential depletion according  
706 to the order of decreasing energy yield for  $C_{\text{org}}$  oxidation, which are not sharply separated in  
707 most aquatic sediments due to, e.g., sediment heterogeneity and mixing resulting from  
708 bioirrigation, bioturbation, and bottom turbidity currents. High benthic mineralization  
709 resulting from the high organic carbon content in the sediment implied that the UB is a  
710 biogeochemical hotspot where significant turnover of organic matter and nutrient  
711 regeneration occur. Over the last 30 years, the gradual deoxygenation and warming of the  
712 bottom water of the East Sea have resulted in an  $\sim 10\%$  decrease in dissolved oxygen and  
713  $\sim 0.04\ ^\circ\text{C}$  increase in potential temperature. If this continues, the UB sediment provides with  
714 an ideal natural laboratory to monitor changes in the rates and partitioning of  $C_{\text{org}}$  oxidation in  
715 order to better understand the biogeochemical cycling of carbon, nutrients and metals  
716 associated with long-term climatic changes.

717

## 718 **Author contribution**

719

720 J-H Hyun as first author and leader of the Korean research group designed the original  
721 experiments and conducted most writing; S-H Kim, JS Mok, and H-Y Cho participated in

722 onboard research activities and analytical processes; V Vandieken participated in onboard  
723 research and was actively involved in the discussion of the manuscript; D Lee, as project  
724 manager of the EAST-1 program, paid the ship-time and has participated in discussion of the  
725 results; B Thamdrup, as leader of the Danish research group, collaborated with J-H Hyun in  
726 designing the experiments and writing and discussing the manuscript.

727

## 728 **Acknowledgements**

729 This research was a part of the projects titled Korean Long-term Marine Ecological  
730 Researches (K-LTMER) and East Asian Seas Time Series-I (EAST-I) funded by the Korean  
731 Ministry of Oceans and Fisheries, and was also supported by the National Research  
732 Foundation of Korea (NRF-2012-013-2012S1A2A1A01030760) in collaboration with the  
733 Danish Council for Independent Research and the Danish National Research Foundation  
734 (DNRF53).

735

## 736 **References**

737

- 738 Aller, R. C. : Bioturbation and manganese cycling in hemipelagic sediments, *Phil. Trans. R.*  
739 *Soc. Lond. A* 331, 51-68, 1990.
- 740 Aller, R. C., Hall, P. O. J., Rude, P. D., and Aller, J. Y. : Biogeochemical heterogeneity and  
741 suboxic diagenesis in hemipelagic sediments of the Panama Basin, *Deep-Sea Res. I*, 45,  
742 133-165, 1998.
- 743 Belkin, I. M. : Rapid warming of Large Marine Ecosystems, *Prog. Oceanogr.*, 81, 207-213,  
744 2009.
- 745 Berg, P., Risgaard-Petersen, N., and Rysgaard, S. : Interpretation shelf and slope: A  
746 comparison of *in situ* microelectrode and chamber flux measurements, *Limnol. Oceanogr.*,  
747 37, 614-629, 1998.
- 748 Boudreau, B. P. : Is burial velocity a master parameter for bioturbation?, *Geochim.*  
749 *Cosmochim. Acta*, 58, 1243-1249, 1994.
- 750 Bowles, M. W., Mogollón, J. M., Kasten, S., Zabel, M., and Hinrichs, K.U. : Global rates of  
751 marine sulfate reduction and implications for sub-sea-floor metabolic activities, *Science*,  
752 344, 889-891, 2014.

753 Broecker, W. S. : The great ocean conveyor, *Oceanogr.*, 4, 79-89, 1991.

754 Broecker, W. S. and Peng, T. H. : Tracers in the sea, Lamont-Doherty Earth Observatory,  
755 Palisades, NY., 1982.

756 Burdige, D. J. and Nealson, K. H. : Chemical and microbiological studies of sulfide-mediated  
757 manganese reduction, *Geomicrobiol. J.*, 4, 361-387, 1986.

758 Canfield, D. E., Jørgensen, B. B., Fossing, H., Glud, R., Gundersen, J., Rasing, N. B.,  
759 Thamdrup, B., Hansen, J. W., Nielsen, L. P., and Hall, P. O. J. : Pathways of organic  
760 carbon oxidation in three continental margin sediments, *Mar. Geol.*, 113, 27-40, 1993a.

761 Canfield, D. E., Thamdrup, B., and Hansen, J. W. : The anaerobic degradation of organic  
762 matter in Danish coastal sediments: iron reduction, manganese reduction, and sulfate  
763 reduction, *Geochim. Cosmochim. Acta*, 57, 3867-3883, 1993b.

764 Canfield, D. E., Thamdrup, B., and Kristensen, E. (Eds.) : Aquatic geomicrobiology, Elsevier,  
765 San Diego, 640 pp., 2005.

766 Cha, H. J., Choi, M. S., Lee, C.-B., and Shin, D.-H. : Geochemistry of surface sediments in  
767 the southwestern East/Japan Sea, *J. Asian Earth Sci.*, 29, 685-697, 2007.

768 Cha, H. J., Lee, C. B., Kim, B. S., Choi, M. S., and Ruttenger, K. C. : Early diagenetic  
769 redistribution and burial of phosphorus in the sediments of the southwestern East Sea  
770 (Japan Sea), *Mar. Geol.*, 216, 127-143, 2005.

771 Cha, H. J. : Geochemistry of surface sediments and diagenetic redistribution of phosphorus in  
772 the southwestern East Sea, PhD thesis, Seoul National Univ., Seoul, Korea, 190 pp., 2002.

773 Choi, Y. J., Kim, D. S., Lee, T. H., and Lee, C. B. : Estimate of manganese and iron oxide  
774 reduction rates in slope and basin sediments of Ulleung Basin, East Sea, *J. Korean Soc.*  
775 *Oceanogr.*, 14, 127-133, 2009.

776 Chough, S. K., Lee, H. J., and Yoon, S. H. (Eds.) : Marine Geology of Korean Seas (2nd  
777 edition), Elsevier, Amsterdam, 2000.

778 Cline, J. D. : Spectrophotometric determination of hydrogen sulfide in natural waters, *Limnol.*  
779 *Oceanogr.*, 14, 454-458, 1969.

780 D'Hondt, S., Inagaki, F., Zarikian, C. A., Abrams, L. J., Dubois, N., Engelhardt, T., Evans,  
781 H., Ferdelman, T., Gribsholt, B., Harris, R. N., Hoppie, B. W., Hyun, J.-H. et al. :  
782 Presence of oxygen and aerobic communities from sea floor to basement in deep-sea  
783 sediments, *Nature Geosci*, 8, 299-304, 2015.

784 Ferdelman, T. G., Fossing, H., Neumann, K., and Schulz, H. D. : Sulfate reduction in surface  
785 sediments of the southeast Atlantic continental margin between 15°38'S and 27°57'S



786 (Angola and Namibia), *Limnol. Oceanogr.*, 44, 650-661, 1999.

787 Fossing, H., Ferdelman, T. G., and Berg, P. : Sulfate reduction and methane oxidation in  
788 continental margin sediments influenced by irrigation (South-East Atlantic off Namibia),  
789 *Geochim. Cosmochim. Acta*, 64, 897-910, 2000.

790 Fossing, H. and Jørgensen, B. B. : Measurement of bacterial sulfate reduction in sediments:  
791 evaluation of a single-step chromium reduction method, *Biogeochem.* 8, 205-222, 1989.

792 Froelich, P. N., Klinkhammer, G.P., Bender, M.L., Luedtke, N.A., Heath, G.R., Cullen, D.,  
793 Dauphin, P., Hammond, D., Hartman, B., and Maynard, V. : Early oxidation of organic  
794 matter in pelagic sediments of the eastern equatorial Atlantic: suboxic diagenesis,  
795 *Geochim. Cosmochim. Acta*, 43, 1075-1090, 1979.

796 Gamo, T. : Dissolved oxygen in the bottom water of the Sea of Japan as a sensitive alarm for  
797 global climatic change, *Trend Anal.Chem.*, 30, 1308-1319, 2011.

798 Gamo, T., Nakayama, N., Takahata, N., Sano, Y., Zhang, J., Yamazaki, E., Taniyasu, S., and  
799 Yamashita, N. : The Sea of Japan and its unique chemistry revealed by time-series  
800 observations over the last 30 Year, *Monogr. Environ. Earth Planets*, 2, 1-22, 2014.

801 Gingele, F. X. and Kasten, S. : Solid-phase manganese in Southeast Atlantic sediments  
802 Implications for the paleoenvironment, *Mar. Geol.*, 121, 317-332, 1994.

803 Glud, R. N. : Oxygen dynamics of marine sediments, *Mar. Biol. Res.*, 4, 243-289, 2008.

804 Gobeil, C, Macdonald, R. W.,and Sundby, B. : Diagenetic separation of cadmium and  
805 manganese in suboxic continental margin sediments, *Geochim. Cosmochim. Acta*, 61,  
806 4647-4654, 1997.

807 Gribsholt, B., Kostka, J. E., and Kristensen, E. : Impact of fiddler crabs and plant roots on  
808 sediment biogeochemistry in a Georgia saltmarsh, *Mar. Ecol. Prog. Ser.*, 259, 237-251,  
809 2003.

810 Haese, R. R., Schramm, J., Rutgers Van Der Loeff, M. M., and Schulz, H. D. : A  
811 comparative study of iron and manganese diagenesis in continental slope and deep  
812 seabasins sediments off Uruguay (SW Atlantic), *Int. J. EarthSci.*, 88, 619-629, 2000.

813 Hall, P. O. and Aller, R.C. : Rapid small-volume, flow injection analysis for CO<sub>2</sub> and NH<sub>4</sub><sup>+</sup> in  
814 marine and freshwaters, *Limnol. Oceanogr.*, 37, 113-119, 1992.

815 Hansen, C., Zabel, M., and Schulz, H. N. : Benthic cycling of oxygen, nitrogen, and  
816 phosphorus, in: *Marine Geochemistry*, edited by: Schulz, H. D. and Zabel, M., Springer-  
817 Verlag, Berlin, Heidelberg, NY, 207-240, 2006.

818 Hansen, J. W., Thamdrup, B., and Jørgensen, B. B. : Anoxic incubation of sediment in gas-

819 tight plastic bags: a method for biochemical process studies, *Mar. Ecol. Prog. Ser.*, 208,  
820 273-282, 2000.

821 Hines, M. E., Bzylinski, D. A., Tugel, J. B., and Lyons, W. B. : Anaerobic microbial  
822 biogeochemistry in sediments from two basins in the Gulf of Maine: evidence for iron and  
823 manganese reduction, *Estuar. Coast. Shelf Sci.*, 32, 313-324, 1991.

824 Hyun, J.-H., Kim, D., Shin, C.-W., Noh, J.-H., Yang, E.-J., Mok, J.-S., Kim, S.-H., Kim, H.-  
825 C., and Yoo, S. : Enhanced phytoplankton and bacterioplankton production coupled to  
826 coastal upwelling and an anticyclonic eddy in the Ulleung basin, East Sea, *Aquat. Microb.  
827 Ecol.*, 54, 45-54, 2009a.

828 Hyun, J.-H., Mok, J.-S., Cho, H.-Y., Kim, S.-H., and Kostka, J. E. : Rapid organic matter  
829 mineralization coupled to iron cycling in intertidal mud flats of the Han River estuary,  
830 Yellow Sea, *Biogeochem.*, 92, 231-245, 2009b.

831 Hyun, J.-H., Mok, J.-S., You, O.-R., Kim, D., and Choi, D. L.: Variations and controls of  
832 sulfate reduction in the continental slope and rise of the Ulleung basin off the southeast  
833 Korean upwelling system in the East Sea, *Geomicrobiol. J.*, 27, 1-11, 2010.

834 Hyun, J.-H., Smith, A. C., and Kostka, J. E. : Relative contributions of sulfate- and iron(III)  
835 reduction to organic matter mineralization and process controls in contrasting habitats of  
836 the Georgia saltmarsh, *Appl. Geochem.*, 22, 2637-2651, 2007.

837 Jahnke, R. A., Reimers, C. E., and Craven, D. B. : Intensification of recycling of organic  
838 matter at the sea floor near ocean margins, *Nature*, 348, 50-54, 1990.

839 Jahnke, R. A. and Jahnke, D. B. : Rates of C, N, P and Si recycling and denitrification at the  
840 US mid-Atlantic continental slope depocenter, *Deep-Sea Res. I*, 47, 1405-1428, 2000.

841 Jahnke, R. A., Emerson, S. R., and Murray, J. W. : A model of oxygen reduction,  
842 denitrification, and organic matter mineralization in marine sediments, *Limnol. Oceanogr.*,  
843 27, 610-623, 1982.

844 Jensen, M. M., Thamdrup, B., Rysgaard, S., Holmer, M., and Fossing, H. : Rates and  
845 regulation of microbial iron reduction in sediments of the Baltic-North Sea transition,  
846 *Biogeochem.*, 65, 295-317, 2003.

847 Jørgensen, B. B. and Kasten, S. : Sulfur cycling and methane oxidation. in: *Marine  
848 Geochemistry*, edited by: Schulz, H. D. and Zabel, M., Springer-Verlag, Berlin,  
849 Heidelberg, NY, 271-309, 2006.

850 Jørgensen, B. B. : A comparison of methods for the quantification of bacterial sulfate  
851 reduction in coastal marine sediments, 1. Measurement with radiotracer techniques,

852 Geomicrobiol. J., 1, 11–28, 1978.

853 Jørgensen, B. B. : Bacteria and marine biogeochemistry, in: Marine Geochemistry, edited by:  
854 Schulz, H. D. and Zabel, M., Springer-Verlag, Berlin, Heidelberg, NY, 169-206, 2006.

855 Jørgensen, B. B. : Mineralization of organic matter in the sea bed - the role of sulphate  
856 reduction, *Nature*, 296, 643-645, 1982.

857 Jørgensen, B. B. and Revsbech, N. P. : Diffusive boundary layers and the oxygen uptake of  
858 sediments and detritus, *Limnol. Oceanogr.*, 30, 111-122, 1985.

859 Kang, D. J., Lee, D. S., and Kim, K.-R. : The East Sea (Sea of Japan), in: Carbon and nutrient  
860 fluxes in continental margins, edited by: Liu, K.-K., Atkinson, L., Quiñones, R. A., and  
861 Talaue-MaManus, L., Springer-Verlag, Berlin, Heidelberg, 383-394, 2010.

862 Kim K, Kim K.-R., Min, D. H., Volkov, Y., Yoon, J.-H., Takematsu, M. : Warming and  
863 structural changes in the East Sea (Japan) Sea: a clue to future changes in the global  
864 oceans?, *Geophys. Res. Lett.*, 28, 3293-3296, 2001.

865 Kim, D., Choi, M.-S., Oh, H.-Y., Kim, K. H., and Noh, J.-H. : Estimate of particulate organic  
866 carbon export flux using  $^{234}\text{Th}/^{238}\text{U}$  disequilibrium in the southwestern East Sea during  
867 summer, (*The Sea*) *J. Kor. Soc. Oceanogr.*, 14, 1-9, 2009.

868 Kim, D., Yang, E.J., Kim, K. H., Shin, C.-W., Park, J., Yoo, S. J., and Hyun, J.-H. : Impact of  
869 an anticyclonic eddy on the summer nutrient and chlorophyll a distributions in the Ulleung  
870 Basin, East Sea (Japan Sea), *ICES J. Marine Science*, 69, 23-29, 2012.

871 Kostka, J. E., Gribsholt, B., Petrie, E., Dalton, D., Skelton, H., and Kristensen, E. : The rates  
872 and pathways of carbon oxidation in bioturbated saltmarsh sediments, *Limnol. Oceanogr.*,  
873 47, 230-240, 2002a.

874 Kostka, J. E., Roychoudhury, A., and Van Cappellen, P. : Rates and controls of anaerobic  
875 microbial respiration across spatial and temporal gradients in saltmarsh sediments,  
876 *Biogeochem*, 60, 49–76, 2002b.

877 Kostka, J. E., Thamdrup, B., Glud, R. N., and Canfield, D. E. : Rates and pathways of carbon  
878 oxidation in permanently cold Arctic sediments, *Mar. Ecol. Prog. Ser.*, 180, 7-21, 1999.

879 Kostka, J. E., Luther, G. W., and Nealson, K. H. : Chemical and biological reduction of  
880 Mn(III)-pyrophosphate complexes – potential importance of dissolved Mn(III) as an  
881 environmental oxidant, *Geochim. Cosmochim. Acta*, 59, 885-894, 1995.

882 Lee, J. S., An, S.-U., Park, Y.-G., Kim, E., Kim, D., Kwon, J. N., Kang, D.-J., and Noh, J.-H. :  
883 Rates of total oxygen uptake of sediments and benthic nutrient fluxes measured using an  
884 in situ autonomous benthic chamber in the sediment of the slope off the southwestern part

885 of the Ulleung Basin, East Sea, *Ocean Sci. J.*, 50, 581-588, 2015.

886 Lee, J.: Importance of nitrate reduction in coastal and deep-sea sediments, MS thesis,  
887 Department of Marine Science Graduate School, Pusan National University, Korea, 86 pp.,  
888 2009.

889 Lee, T., Hyun, J.-H., Mok, J. S., and Kim, D. : Organic carbon accumulation and sulfate  
890 reduction rates in slope and basin sediments of the Ulleung basin, East/Japan Sea, *Geo.*  
891 *Mar. Lett.* 28, 153-159, 2008.

892 Li, Y. H. and Gregory, S. : Diffusion of ions in sea water and deep sea sediments. *Geochim.*  
893 *Cosmochim. Acta*, 38, 703-714, 1974.

894 Liu, K.-K., Atkinson, L., Quiñones, R. A., and Talaue-MaManus, L. : Biogeochemistry of the  
895 continental margins, in: Carbon and nutrient fluxes in continental margins, edited by: Liu,  
896 K.-K., Atkinson, L., Quiñones, R. A., and Talaue-MaManus, L., Springer-Verlag, Berlin,  
897 Heidelberg, 3-24, 2010.

898 Lovley, D. R. and Phillips, E. J. P. : Competitive mechanisms for inhibition of sulfate  
899 reduction and methane production in the zone of ferric iron reduction in sediments, *Appl.*  
900 *Environ. Microbiol.*, 53, 2636-2641, 1987.

901 Lovley, D. R. and Phillips, E. J. P. : Manganese inhibition of microbial iron reduction in  
902 anaerobic sediments, *Geomicrobiol. J.*, 6, 145-155, 1988.

903 Luther III, G. W. : Acid volatile sulfide – A comment, *Mar. Chem.*, 97, 198-205, 2005.

904 Macdonald, R. W. and Gobeil, C. : Manganese sources and sinks in the Arctic Ocean with  
905 reference to periodic enrichments in basin sediments, *Aquat. Geochem.*, 18, 565-591, 2012.

906 Madison, S., Tebo, B. M., Mucci, A., Sundby, B., and Luther III, G. W. : Abundant  
907 porewater Mn(III) is a major component of the sedimentary redox system, *Science*, 341,  
908 875-878, 2013.

909 Magen, C., Mucci, A., and Sundby, B. : Reduction rates of sedimentary Mn and Fe oxides: an  
910 incubation experiment with Arctic Ocean sediments, *Aquat. Biogeochem.*, 17, 629-643,  
911 2011.

912 Melton, E. D., Swanner, E. D., Behrens, S., Schmidt, C., and Kappler, A. : The interplay of  
913 microbially mediated and abiotic reactions in the biogeochemical Fe cycle, *Nature Rev.*  
914 *Microbiol.*, 12, 797-808, 2014.

915 Mewes, K., Mogollón, J. M., Picard, A., Rühlemann, C., Eisenhauer, A., Kuhn, T., Ziebis, W.,  
916 and Kasten, S. : Diffusive transfer of oxygen from seamount basaltic crust into overlying  
917 sediments: an example from the Clarion-Clipperton Fracture Zone, *Earth Planet. Sci. Lett.*,

918 433, 215-225, 2016.

919 Mewes, K., Mogollón, J. M., Picard, A., Rühlemann, C., Kuhn, T., Nöthen, K., and Kasten,  
920 S. : Impact of depositional and biogeochemical processes on small scale variations in  
921 nodule abundance in the Clarion-Clipperton Fracture Zone, *Deep-Sea Res. I*, 91, 125-141,  
922 2014.

923 Meyers, C. and Nealson, K. H.: Microbial reduction of manganese oxides: Interactions with  
924 iron and sulfur, *Geochim. Cosmochim. Acta*, 52, 2727-2732, 1988.

925 Mogollón, J. M., Mewes, K., and Kasten, S. : Quantifying manganese and nitrogen cycle  
926 coupling in manganese-rich, organic carbon-starved marine sediments: examples from the  
927 Clarion-Clipperton fracture zone, *Geophys. Res. Lett.*, 43, doi:10.1002/2016GL069117,  
928 2016.

929 Mouret, A., Anschutz, P., Lecroart, P., Chaillou, G., Hyacinthe, C., Deborde, J., Jorissen,  
930 F., Deflandre, B., Schmidt, S., and Jouanneau, J.-M. : Benthic geochemistry of manganese  
931 in the Bay of Biscay, and sediment mass accumulation rate, *Geo. Mar. Lett.* 29, 133-149,  
932 2009.

933 Murray, J. W., Balistrieri, L. S., and Paul, B. : The oxidation state of manganese in  
934 marine sediments and ferromanganese nodules, *Geochim. Cosmochim. Acta*, 48, 1237-  
935 1247, 1984.

936 Nickel, M., Vandieken, V., Brüchert, V., and Jørgensen, B. B. : Microbial Mn(IV) and Fe(III)  
937 reduction in northern Barents Sea sediments under different conditions of ice cover and  
938 organic carbon deposition, *Deep-Sea Res. II*, 55, 2390-2398, 2008.

939 Parsons, T. R., Maita, Y., and Lalli, C. M. (Eds.) : A manual of chemical and biological  
940 methods for seawater analysis, Pergamon Press, Oxford, 173 pp., 1984.

941 Phillips, E. J. P. and Lovley, D. R. : Determination of Fe(III) and Fe(II) in oxalate extracts of  
942 sediment, *Soil Sci. Soc. Am. J.*, 51, 938-941, 1987.

943 Postma, D. : Concentration of Mn and separation from Fe in sediments – I. Kinetics and  
944 stoichiometry of the reaction between birnessite and dissolved Fe(II) at 10°C, *Geochim.*  
945 *Cosmochim. Acta*, 49, 1023-1033, 1985.

946 Pyzik, A. E. and Sommer, S. E. : Sedimentary iron monosulfide: kinetics and mechanisms of  
947 formation, *Geochim. Cosmochim. Acta*, 45, 687-698, 1981.

948 Rasmussen, H. and Jørgensen, B. B. : Microelectrode studies of seasonal oxygen uptake in a  
949 coastal sediment: role of molecular diffusion, *Mar. Ecol. Prog. Ser.*, 81, 289-303, 1992.

950 Rickard, D. and Morse, J. W. : Acid volatile sulfur (AVS), *Mar. Chem.*, 97, 141-107, 2005.

951 Romankevich, E. A. : Geochemistry of organic matter in the ocean, Springer-Verlag, Berlin,  
952 Heidelberg, NY, Tokyo, 334 pp., 1984.

953 Schaller, T. and Wehrli, B. : Geochemical-focusing of manganese in lake sediments –An  
954 indicator of deep-water oxygen conditions, *Aquat. Geochem.*, 2, 359-378, 1997.

955 Slomp, C. P., Mort, H. P., Jilbert, T., Reed, D. C., and Gustafsson, B. G. : Coupled dynamics  
956 of iron and phosphorus in sediments of an oligotrophic coastal basin and the impact of  
957 anaerobic oxidation of methane, *PLoS ONE*, 8, e62386, 2013.

958 Sørensen, J. W. and Jørgensen, B. B. : Early diagenesis in sediments from Danish coastal  
959 waters: Microbial activity and Mn-Fe-S geochemistry, *Geochim. Cosmochim. Acta*, 51,  
960 1583-1590, 1987.

961 Sørensen, J. W., Jørgensen, B. B., and Revsbech, N. P. : A comparison of oxygen, nitrate and  
962 sulfate respiration in a coastal marine sediment, *Microb. Ecol.*, 5, 105-115, 1979.

963 Stookey, L. L. : Ferrozine - a new spectrophotometric reagent for iron, *Anal. Chem.* 42, 779-  
964 781, 1970.

965 Sundy, B. and Silverberg, N. : Manganese fluxes in the benthic boundary layer, *Limnol.*  
966 *Oceanogr.*, 30, 372-381, 1985.

967 Thamdrup, B. and Canfield, D. E. : Pathways of carbon oxidation in continental margin  
968 sediments off central Chile, *Limnol. Oceanogr.* 41, 1629-1650, 1996.

969 Thamdrup, B. and Dalsgaard, T. : The fate of ammonium in anoxic manganese oxide-rich  
970 marine sediment, *Geochim. Cosmochim. Acta*, 64, 4157-4164, 2000.

971 Thamdrup, B., Rosselló-Mora, R., and Amann, R. : Microbial manganese and sulfate  
972 reduction in Black Sea shelf sediments, *Appl. Environ. Microbiol.*, 66, 2888-2897, 2000.

973 Thamdrup, B. : Bacterial manganese and iron reduction in aquatic sediments, *Adv. Microb.*  
974 *Ecol.* 16, 41-84, 2000.

975 Trimmer, M. and Engström, P. : Distribution, activity, and ecology of anammox bacteria in  
976 aquatic environments, in: *Nitrification*, edited by: Ward, B. B., Arp, D. J., and Klotz, M. G.,  
977 ASM Press, Washington, DC, 201-235, 2011.

978 Trimmer, M., Engström, P., and Thamdrup, B. : Stark contrast in denitrification and anammox  
979 across the deep Norwegian Trench in the Skagerrak, *Appl. Environ. Microbiol.*, 79, 7381-  
980 7389, 2013.

981 Vandieken, V., Pester, M., Finke, N., Hyun, J.-H., Friedrich, M. W., Loy, A., and Thamdrup,  
982 B. : Identification of acetate-oxidizing manganese-reducing bacteria in three manganese  
983 oxide-rich marine sediments by stable isotope probing, *ISME J.*, 6, 2078-2090, 2012.

- 984 Vandieken, V., Finke, N., and Thamdrup, B. : Hydrogen, acetate, and lactate as electron  
985 donors for microbial manganese reduction in a manganese-rich coastal marine sediment,  
986 FEMS Microbiol Ecol., 87, 733-745, 2014.
- 987 Vandieken, V., Nickel, M., and Jørgensen, B. B. : Carbon mineralization in Arctic sediments  
988 northeast of Svalbard: Mn(IV) and Fe(III) reduction as principal anaerobic respiratory  
989 pathways, Mar. Ecol. Prog. Ser., 322, 15-27, 2006.
- 990 Walsh, J. J. : Importance of continental margins in the marine biogeochemical cycling of  
991 carbon and nitrogen, Nature, 350, 53-55, 1991.
- 992 Yamada, K., Ishizaka, J., and Nagata, H. : Spatial and temporal variability of satellite primary  
993 production in the Japan Sea from 1998 to 2002, J. Oceanogr., 61, 857-869, 2005.
- 994 Yin, J. H., Kajiwara, Y., and Fujii, T. : Distribution of transition elements in surface  
995 sediments of the southwestern margin of Japan Sea. Geochem. J., 23, 161-180, 1989.
- 996 Yoo, S. and Park, J. S. : Why is the southwest the most productive region of the East Sea/Sea  
997 of Japan?, J. Mar. Syst., 78, 301-315, 2009.

998

999 Table 1. Environmental settings and sediment characteristics

Environmental parameter	M1 (Continental slope)	D3 (Center of the basin)
Latitude	36° 10' N	37° 00' N
Longitude	130° 10' E	131° 00' E
Water depth (m)	1,453	2,154
Sediment temperature (°C)	1.3	0.6
Pore-water salinity (psu)	34.2	34.8
Water content (%)	85 (± 3.1)	77 (± 1.8)
Porosity	0.95 (± 0.03)	0.86 (± 0.01)
Density (g cm <sup>-3</sup> )	1.10 (± 0.02)	1.12 (± 0.02)
Total organic carbon (% , dry wt.)	3.96 (± 0.27)	2.66 (± 0.09)
Total organic nitrogen (% , dry wt.)	0.38 (± 0.01)	0.35 (± 0.01)

1000 Numbers in parenthesis indicate ± 1SD of triplicate samples.

1001

1002



1003  
1004  
1005  
1006

Table 2. Oxygen penetration depth (OPD), diffusive oxygen utilization (DOU) rate and O<sub>2</sub> consumption rate by aerobic respiration and re-oxidation of reduced inorganic compounds (RIC) in the pore water.

Station	OPD (mm)	DOU (mmol O <sub>2</sub> m <sup>-2</sup> d <sup>-1</sup> )	O <sub>2</sub> consumption (mmol O <sub>2</sub> m <sup>-2</sup> d <sup>-1</sup> ) by	
			Aerobic respiration	Re-oxidation of RIC
M1	3.2 (± 0.20)	7.12 (± 1.36)	4.04 (± 2.03)	3.07 (± 0.68)
D3	3.6 (± 0.03)	5.95 (± 0.16)	2.53 (± 0.72)	3.42 (± 0.58)

1007  
1008  
1009  
1010

Values represent averages ± 1SD (*n* = 3)

1011 Table 3. Depth integrated rates ( $\text{mmol m}^{-2} \text{d}^{-1}$ ) of Mn reduction, Fe reduction, and sulfate reduction and the partitioning of abiotic and  
 1012 microbial Fe(III) reduction in total Fe(III) reduction with depth.

St.	Depth Interval (cm)	$\text{SO}_4^{2-}$ Red	Mn Red	<sup>(a)</sup> Total Fe(III) Red	Fe reduction by		Fe Red <sub>(Microbial)</sub> / Fe Red <sub>(Abiotic)</sub>
					<sup>(a)</sup> Abiotic Fe Red	<sup>(a)</sup> Microbial Fe Red	
M1	0 – 2	1.35	0.04	4.75	0.90	3.86	4.28
	2 – 4	1.04	-	3.02	0.70	2.33	3.33
	4 – 6	0.84	-	1.58	0.56	1.21	2.16
	6 – 8	0.54	-	1.25	0.36	0.89	2.47
	8 – 10	0.53	-	0.77	0.36	0.41	1.14
	Sum (0-10)	4.30	0.04	11.4	2.88	8.70	
D3	0 – 2	0.06	<sup>(b)</sup> 3.19	-	-	-	n.a.
	2 – 4	0.11	3.96	1.63	0.07	1.56	22.3
	4 – 6	0.13	1.05	4.80	0.09	4.71	52.3
	6 – 8	0.06	0.01	0.86	0.04	0.83	20.8
	8 – 10	0.07	0.00	0.24	0.05	0.19	3.80
	Sum (0-10)	0.43	8.21	7.53	0.25	7.29	

1013 <sup>(a)</sup>Stoichiometric equations were used to evaluate the relative significance of abiotic and microbial Fe reduction:

1014 Abiotic reduction of Fe(III) by sulfide oxidation,  $3\text{H}_2\text{S} + 2\text{FeOOH} = 2\text{FeS} + \text{S}^0 + 4\text{H}_2\text{O}$ ; Microbial Fe(III) reduction = Total Fe(III) reduction – abiotic Fe(III) reduction.

1015 <sup>(b)</sup>back-calculated from the C oxidation by Mn reduction in the 0 – 2 cm interval in Table 5 using the stoichiometric equation,  $2\text{MnO}_2 + \text{CH}_2\text{O} + \text{H}_2\text{O} = 2\text{Mn}^{2+} + \text{HCO}_3^- + 3\text{OH}^-$ .

1016 ‘-’ indicates that the process does not occur or is regarded as negligible at the depth interval based on the OPD for aerobic respiration and geochemical profiles or anoxic  
 1017 bag incubations for Mn(IV) and Fe(III) reduction

1018 ‘n.a.’ indicates that data are not available.

1019

1020

1021

Table 4. Organic carbon ( $C_{org}$ ) oxidation ( $mmol\ C\ m^{-2}\ d^{-1}$ ) by each  $C_{org}$  oxidation pathway, and its partitioning in total  $C_{org}$  oxidation (% Total  $C_{ox}$ ) and anaerobic  $C_{org}$  oxidation (% Anaerobic  $C_{org}\ ox$ ) at each depth interval within 10 cm of the sediment. Mn Red, Mn reduction; Fe Red, Fe reduction; and  $SO_4^{2-}$  Red, sulfate reduction

St.	Depth Interval (cm)	$C_{org}$ oxidation measured by		<sup>(c)</sup> Total $C_{org}$ oxidation (DOU + DIC)	Anaerobic $C_{org}$ oxidation by dissimilatory			Total anaerobic $C_{org}$ oxidation (Mn Red + Fe Red + $SO_4^{2-}$ Red)	Total Anaerobic $C_{org}$ oxidation / Anoxic DIC production
		<sup>(a)</sup> DOU (Aerobic respiration)	<sup>(b)</sup> DIC prod. (Anaerobic respiration)		<sup>(d)</sup> Mn Red	<sup>(d,e)</sup> Fe Red	<sup>(d)</sup> $SO_4^{2-}$ Red		
M1	0 – 2	3.11	5.59	8.70	0.02	0.96	2.69	3.67	0.66
	2 – 4	-	3.31	3.31	-	0.58	2.09	2.67	0.81
	4 – 6	-	2.26	2.26	-	0.26	1.67	1.93	0.85
	6 – 8	-	1.50	1.50	-	0.22	1.08	1.30	0.87
	8 – 10	-	1.37	1.37	-	0.10	1.06	1.17	0.85
	Sum (0 – 10)	3.11	14.0	17.1	0.02	2.13	8.59	10.7	0.77
	(% Total $C_{org}\ ox$ ) (% Anaerobic $C_{org}\ ox$ )	(18.1)	(81.9)	(100)	(0.13)	(12.4)	(50.1)	(62.7)	
D3	0 – 2	1.94	1.72	3.66	<sup>(f)</sup> 1.59	-	0.13	1.72	1.00
	2 – 4	-	2.72	2.72	1.98	0.39	0.22	2.58	0.95
	4 – 6	-	2.32	2.32	0.52	1.18	0.26	1.96	0.84
	6 – 8	-	0.30	0.30	0.01	0.21	0.12	0.33	1.10
	8 – 10	-	0.16	0.16	-	0.05	0.15	0.19	1.21
	Sum (0 – 10)	1.94	7.22	9.2	4.10	1.82	0.86	6.79	0.94
	(% Total $C_{org}\ ox$ ) (% Anaerobic $C_{org}\ ox$ )	(20.6)	(78.8)	(100)	(44.8)	(19.9)	(9.41)	(77.8)	

1022 <sup>(a)</sup> Aerobic  $C_{org}$  oxidation rate (=  $O_2$  consumption by aerobic respiration  $\times$  (106C/138 $O_2$ ) calculated using the Redfield ratio;  $O_2$  consumption by aerobic respiration rate (= DOU - re-oxidation  
1023 rates) is calculated from Table 2 that is derived from the  $O_2$  micro-profiles in Fig. 2.

1024 <sup>(b)</sup> independently measured from the DIC accumulation rate in anoxic bag incubation experiment in Fig. 6 and 7.

1025 <sup>(c)</sup> Total  $C_{org}$  oxidation = aerobic  $C_{org}$  oxidation + anaerobic  $C_{org}$  oxidation

1026 <sup>(d)</sup>  $C_{org}$  oxidation by dissimilatory Mn(IV) reduction, Fe(III) reduction, and sulfate reduction was calculated from the stoichiometric equations:  $2MnO_2 + CH_2O + H_2O = 2Mn^{2+} + HCO_3^- +$   
1027  $3OH^-$ ;  $4Fe(OH)_3 + CH_2O = 4Fe^{2+} + HCO_3^- + 7OH^-$ ;  $SO_4^{2-} + 2CH_2O = H_2S + 2HCO_3^-$ ,  $H_2S = HS^- + H^+$

1028 <sup>(e)</sup> Dissimilatory Fe(III) reduction = (Total Fe(III) reduction in Fig.7) – (Abiotic Fe(III) reduction coupled to  $H_2S$  oxidation;  $3H_2S + 2FeOOH = 2FeS + S^0 + 4H_2O$ )

1029 <sup>(f)</sup> back-calculated from: DIC production rate - ( $C$  oxidation by  $SO_4^{2-}$  Red and Fe Red). See text for further discussion

1030 ‘ - ’ indicates that the process does not occur or is regarded as negligible based on the OPD for aerobic respiration and geochemical profiles or anoxic bag incubations for Mn and Fe Red.

1031

1032

## Figure legends

Fig. 1. Sampling stations in the East Sea and pictures showing contrasting colors between surface sediments of the continental slope (M1) and center of the basin (D3)

Fig. 2. Concentrations of dissolved  $\text{NH}_4^+$ ,  $\text{NO}_3^-$ ,  $\text{Mn}^{2+}$  and  $\text{Fe}^{2+}$  in pore water and contents of solid phase  $\text{Mn}_{(\text{DCA})}$ ,  $\text{Fe(II)}_{(\text{oxal})}$ ,  $\text{Fe(III)}_{(\text{oxal})}$ , acid volatile sulfur (AVS) and chromium reducible sulfur (CRS) in the sediment at M1 and D3.

Fig. 3. Vertical profiles of  $\text{O}_2$ . The slashed area indicates the diffusive boundary layer in the sediment-water interface. The shaded area indicates that  $\text{O}_2$  consumption by aerobic respiration (I and II) and re-oxidation of reduced inorganic compounds (III), respectively.

Fig. 4. Changes of concentrations of DIC,  $\text{Ca}^{2+}$  and  $\text{Mn}^{2+}$  in pore water and contents of solid phase  $\text{Fe(II)}_{(\text{oxal})}$  during anoxic bag incubations of sediments from 0-2, 2-4, 4-6, and 6-8 cm depth at M1 and D3. Data obtained at 8-10 cm depth interval is not shown.

Fig. 5. Vertical distribution of terminal electron acceptors ( $\text{O}_2$ ,  $\text{NO}_3^-$ , Mn and Fe) and rates of sulfate reduction measured from whole core analyses, and rates of anaerobic carbon oxidation (DIC production rates), Mn reduction and Fe reduction measured from anoxic bag incubations in Fig. 4.  $\text{C}_{\text{org}}$  by sulfate reduction in panel C and H was calculated from the stoichiometry of 2:1 of  $\text{C}_{\text{org}}$  oxidized to sulfate reduced.

Fig. 6. Depth variations of partitioning of each carbon oxidation pathway in total carbon oxidation at M1 and D3

Fig. 7. The relative contribution of Mn reduction to anaerobic carbon oxidation as a function of the content of  $\text{Mn}_{(\text{DCA})}$  at 3 different sites. BS, Black Sea (Thamdrup et al. 2000); UB, Ulleung Basin (This study); Sk, Skagerrak (Canfield et al. 1993b).

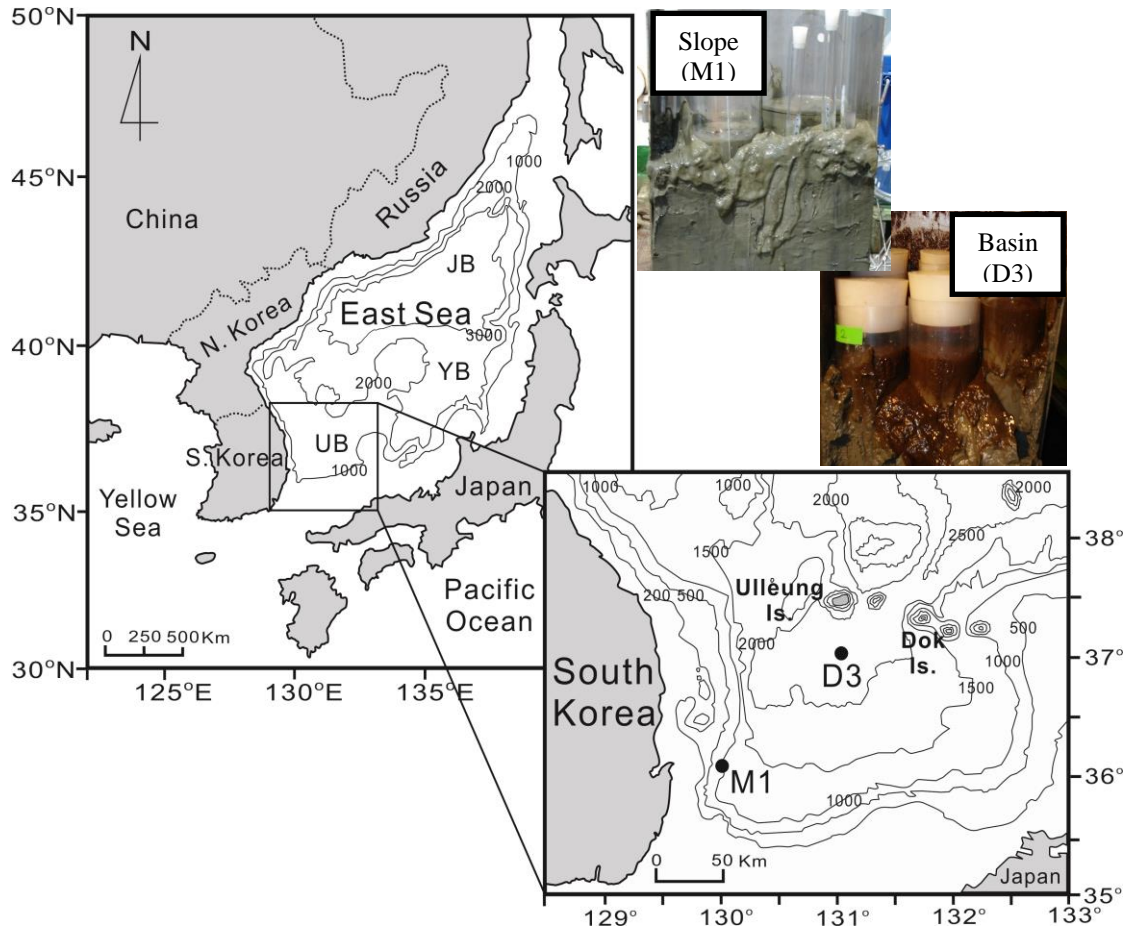
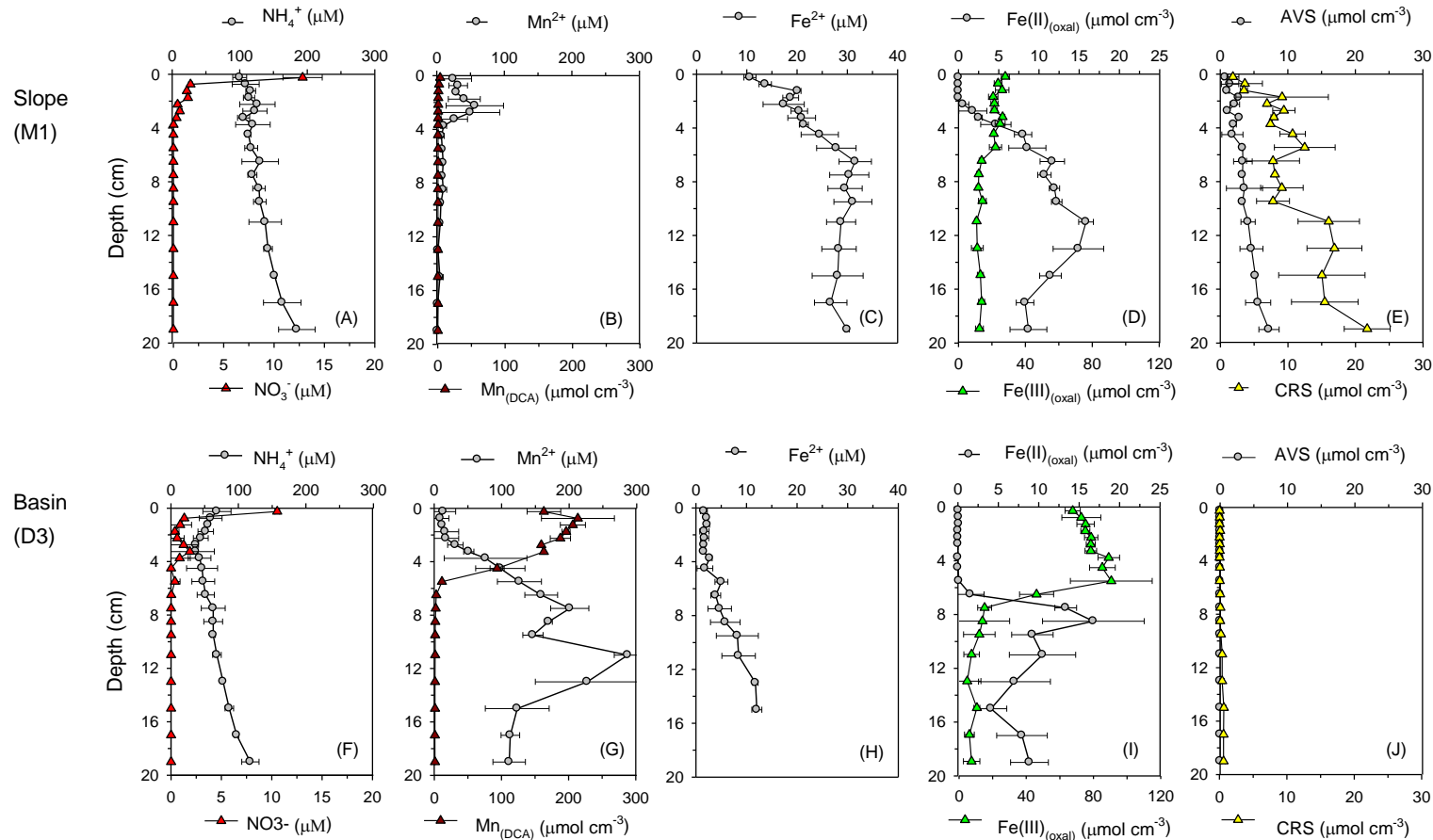


Fig. 1. Sampling stations in the East Sea and pictures showing contrasting colors between surface sediments of the continental slope (M1) and center of the basin (D3)

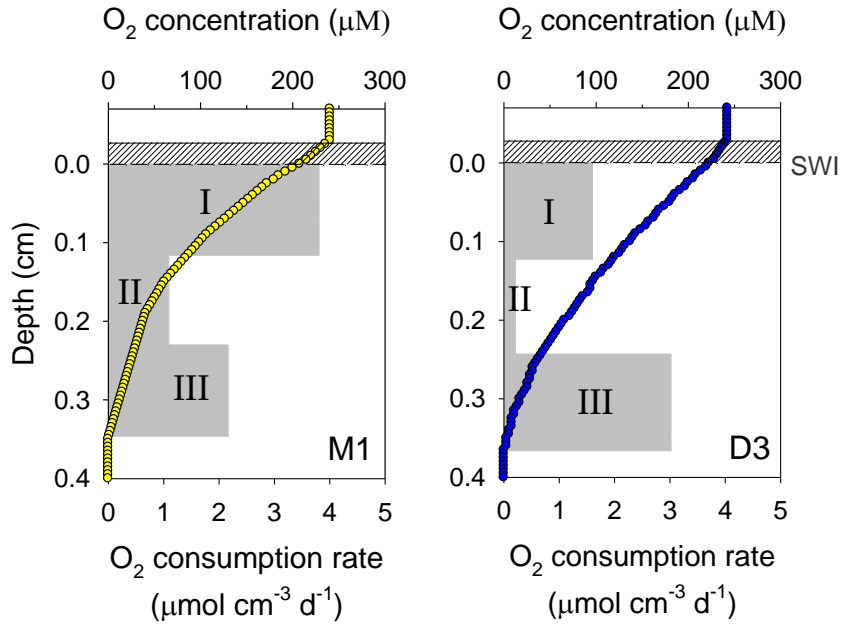
1 Hyun et al – Figure 2



2  
3  
4  
5  
6

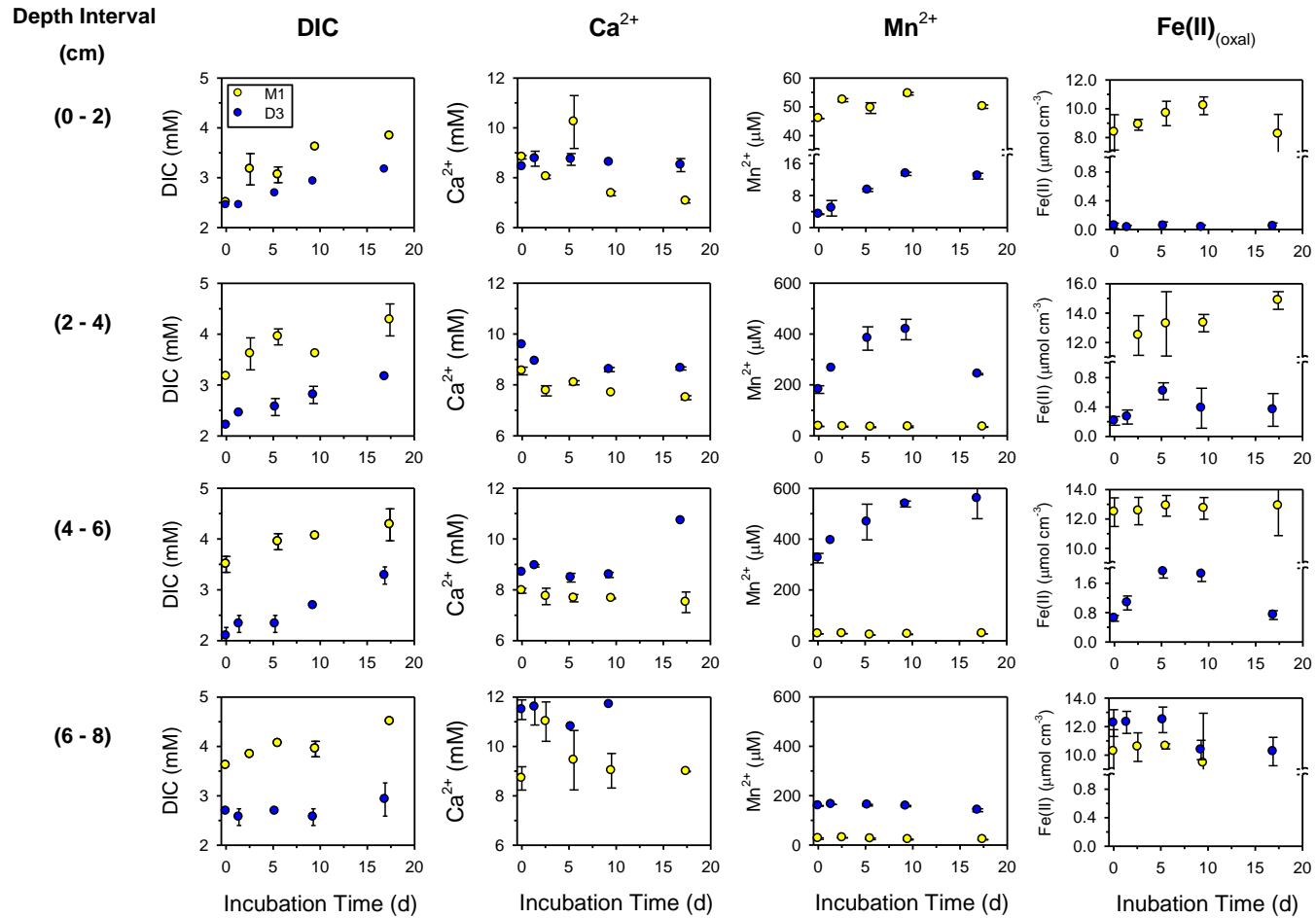
Fig. 2. Concentrations of dissolved  $\text{NH}_4^+$ ,  $\text{NO}_3^-$ ,  $\text{Mn}^{2+}$  and  $\text{Fe}^{2+}$  in pore water and contents of solid phase  $\text{Mn}_{(\text{DCA})}$ ,  $\text{Fe(II)}_{(\text{oxal})}$ ,  $\text{Fe(III)}_{(\text{oxal})}$ , acid volatile sulfur (AVS) and chromium reducible sulfur (CRS) in the sediment at M1 and D3.

7 Hyun et al – Figure 3  
8  
9



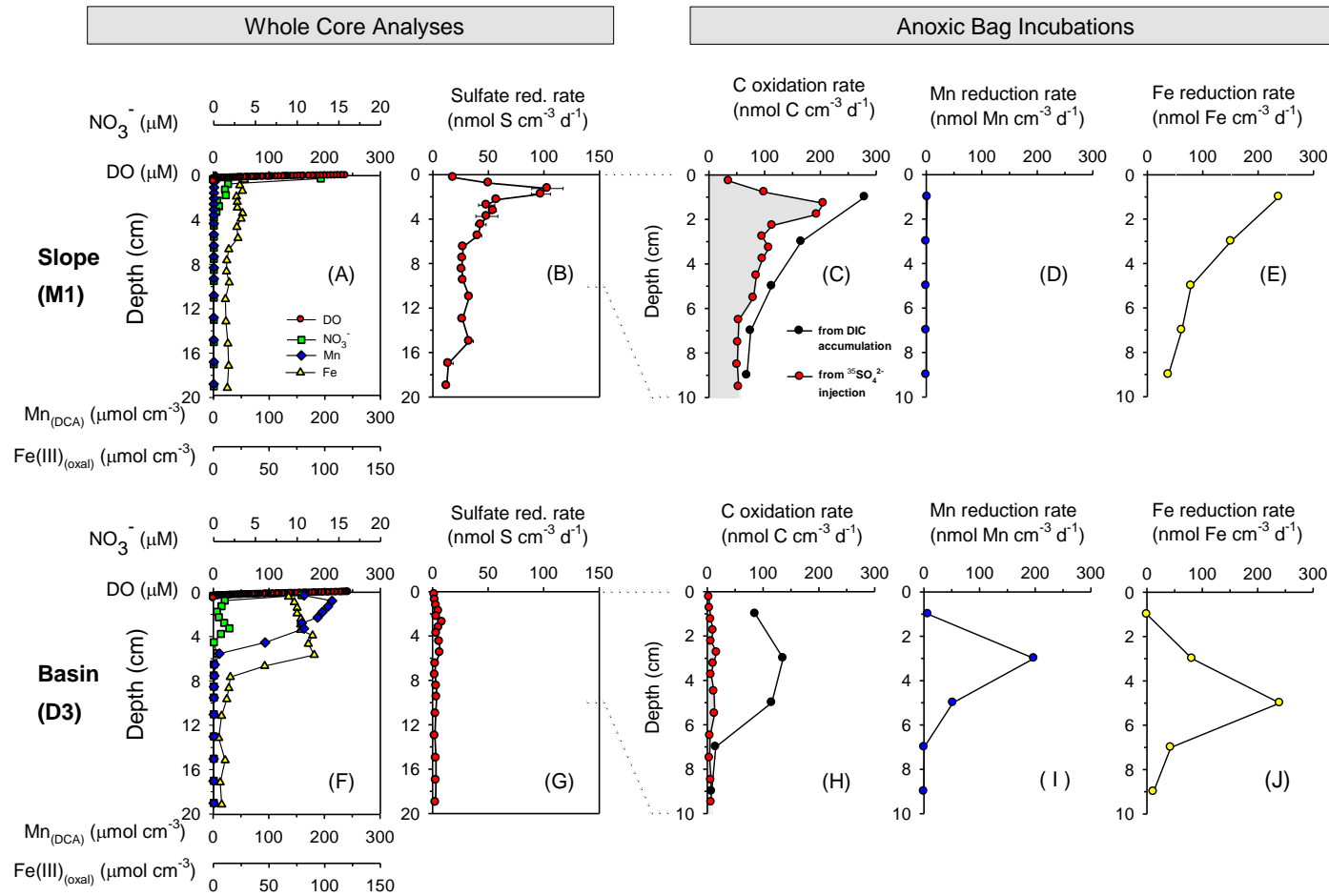
10  
11  
12  
13  
14  
15  
16  
17  
18  
19  
20

Fig. 3. Vertical profiles of O<sub>2</sub> concentration and consumption rate. The slashed area indicates diffusive boundary layer in the sediment-water interface. The shaded area indicates that O<sub>2</sub> consumption by aerobic respiration (I and II) and re-oxidation of reduced inorganic compounds (III), respectively.



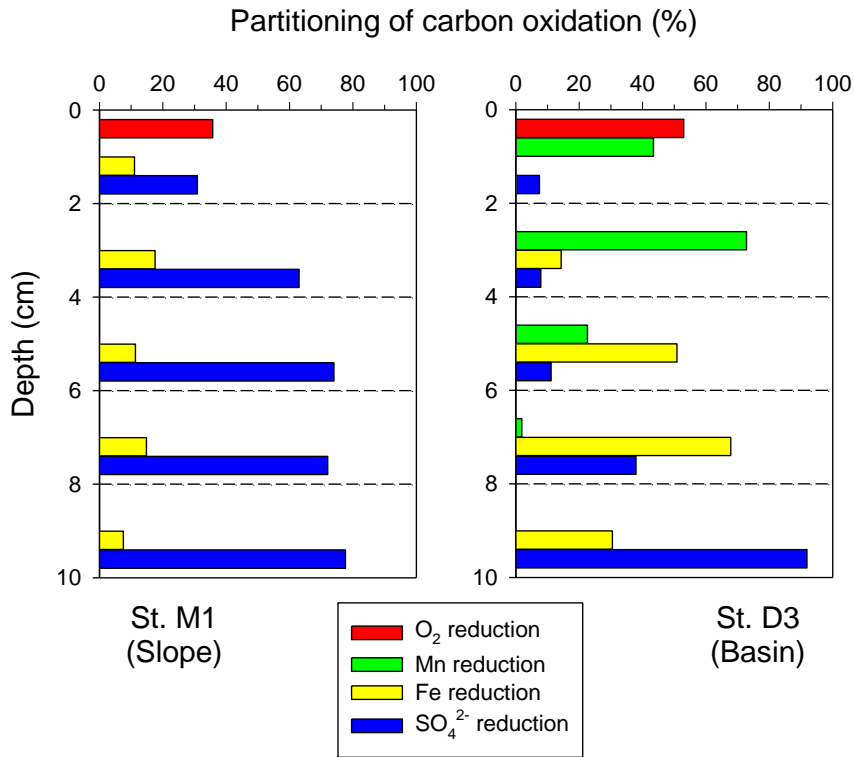
24 Fig. 4. Changes of concentrations of DIC, Ca<sup>2+</sup> and Mn<sup>2+</sup> in pore water and contents of solid phase Fe(II)<sub>(oxal)</sub> during anoxic bag incubations of  
 25 sediments from 0-2, 2-4, 4-6, and 6-8 cm depth at M1 and D3. Data obtained at 8-10 cm depth interval is not shown.





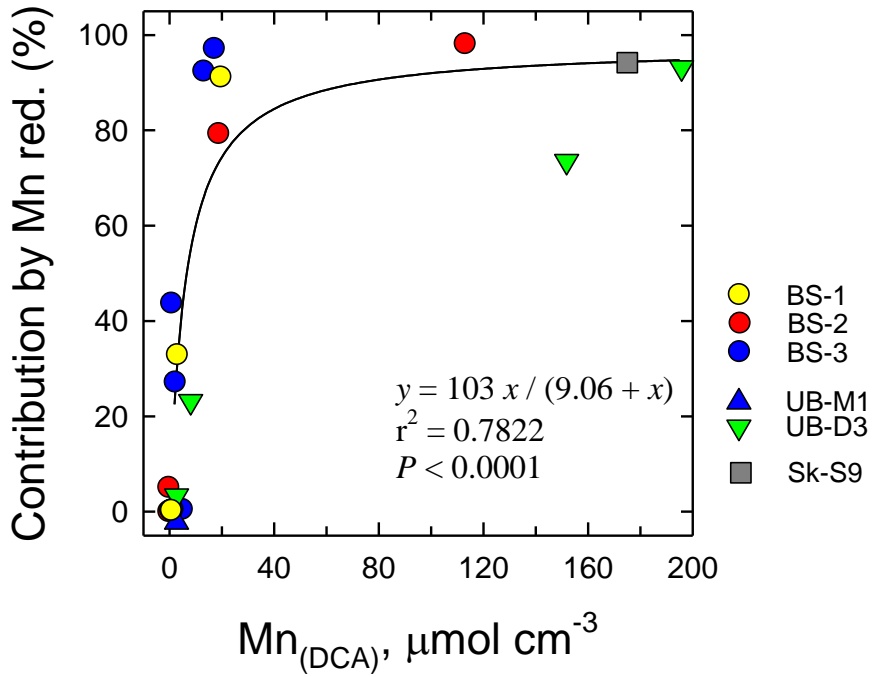
27  
 28 Fig. 5. Vertical distribution of terminal electron acceptors ( $\text{O}_2$ ,  $\text{NO}_3^-$ , Mn and Fe) and rates of sulfate reduction measured from whole core analyses, and  
 29 rates of anaerobic carbon oxidation (DIC production rates), Mn reduction and Fe reduction measured from anoxic bag incubations in Fig. 4.  $\text{C}_{\text{org}}$  by sulfate  
 30 reduction in panel C and H was calculated from the stoichiometry of 2:1 of  $\text{C}_{\text{org}}$  oxidized to sulfate reduced.

31 Hyun et al. – Figure 6  
32  
33



34  
35  
36  
37 Fig. 6. Depth variations of partitioning of each carbon oxidation pathway in total carbon  
38 oxidation at M1 and D3  
39

40  
41 Hyun et al - Figure 7  
42



43  
44  
45  
46  
47  
48  
49

Fig. 7. The relative contribution of Mn reduction to anaerobic carbon oxidation as a function of the content of Mn(DCA) at 3 different sites. BS, Black Sea (Thamdrup et al. 2000); UB, Ulleung Basin (This study); Sk, Skagerrak (Canfield et al. 1993b).